Journal of Zhejiang University-SCIENCE B (Biomedicine & Biotechnology) 2025 26(6):589-608
www.jzus.zju.edu.cn; www.springer.com/journal/11585
E-mail: jzus_b@zju.edu.cn

Research Article

https://doi.org/10.1631/jzus.B2400099

Single-cell transcriptome analysis reveals abnormal angiogenesis and placentation by loss of imprinted glutaminyl-peptide cyclotransferase

Jing GUO[1,2*], Jihong ZHENG[1*], Ruixia LI[3*], Jindong YAO[1], He ZHANG[4], Xu WANG[5,6✉], Chao ZHANG[1✉]

[1]*Fundamental Research Center, Shanghai Yangzhi Rehabilitation Hospital (Shanghai Sunshine Rehabilitation Center), School of Life Sciences and Technology, Tongji University, Shanghai 200092, China*
[2]*Lingang Laboratory, Shanghai Center for Brain Science and Brain-Inspired Intelligence Technology, Shanghai 201306, China*
[3]*Obstetrics & Gynecology Hospital of Fudan University, Fudan University School of Medicine, Shanghai 200433, China*
[4]*Institute for Regenerative Medicine, Shanghai East Hospital, School of Life Science and Technology, Tongji University, Shanghai 200092, China*
[5]*Department of Pathobiology, College of Veterinary Medicine, Auburn University, Auburn, AL 36849, USA*
[6]*HudsonAlpha Institute for Biotechnology, Huntsville, AL 35806, USA*

Abstract: Imprinted genes play a key role in regulating mammalian placental and embryonic development. Here, we generated glutaminyl-peptide cyclotransferase-knockout (*Qpct*$^{-/-}$) mice utilizing the clustered regularly interspaced short palindromic repeats (CRISPR)/CRISPR-associated protein 9 (Cas9) platform and identified *Qpct* as a novel anti-angiogenic factor in regulating mouse placentation. Compared with *Qpct*$^{+/+}$ mice, placentae and embryos (*Qpct*$^{-/+}$ and *Qpct*$^{-/-}$) showed significant overgrowth at embryonic Day 12.5 (E12.5), E15.5, and E18.5. Using single-cell transcriptome analysis of 32 309 cells from *Qpct*$^{+/+}$ and *Qpct*$^{-/-}$ mouse placentae, we identified 13 cell clusters via single-nucleus RNA sequencing (snRNA-seq) (8880 *Qpct*$^{+/+}$ and 13 577 *Qpct*$^{-/-}$ cells) and 20 cell clusters via single-cell RNA sequencing (scRNA-seq) (6567 *Qpct*$^{+/+}$ and 3285 *Qpct*$^{-/-}$ cells). Furthermore, we observed a global up-regulation of pro-angiogenic genes in the *Qpct*$^{-/-}$ background. Immunohistochemistry assays revealed a notable increase in the number of blood vessels in the decidual and labyrinthine layers of E15.5 *Qpct*$^{-/+}$ and *Qpct*$^{-/-}$ mice. Moreover, the elevation of multiple pairs of ligand-receptor interactions was observed in decidual cells, endothelial cells, and macrophages, promoting angiogenesis and inflammatory response. Our findings indicate that loss of maternal *Qpct* leads to altered phenotypic characteristics of placentae and embryos and promotes angiogenesis in murine placentae.

Key words: Glutaminyl-peptide cyclotransferase-knockout (*Qpct*$^{-/-}$) mice; Placenta; Single-cell sequencing; Overgrowth; Angiogenesis

1 Introduction

A cumulative study has identified nearly 200 imprinted genes in the mouse genome (Tucci et al., 2019). In line with the "parental conflict" theory, paternally expressed genes are associated with the enhancement of feto-placental growth, whereas maternally expressed genes function to constrain conceptus development (Fowden et al., 2011; Haig, 2014). Most imprinted genes are associated with reproductive and developmental disorders in mice and humans, such as *H19* (Bartolomei et al., 1991), insulin-like growth factor 2 (*Igf2*), and growth factor receptor-binding protein 10 (*Grb10*) (Charalambous et al., 2010; Garfield et al., 2011; Plasschaert and Bartolomei, 2015). Previous research has demonstrated that various imprinted genes are crucial for embryonic and placental development, primarily through their role in regulating angiogenesis (Miozzo et al., 2001; Torres et al., 2017).

The placenta serves as an essential organ connecting the mother to the developing fetus, playing a key role in controlling growth and development in mammals (Hemberger et al., 2020). Extensive angiogenesis

✉ Xu WANG, xzw0070@auburn.edu
Chao ZHANG, zhangchao@tongji.edu.cn
* The three authors contributed equally to this work
Xu WANG, https://orcid.org/0000-0002-7594-5004
Chao ZHANG, https://orcid.org/0000-0001-6418-8370

Received Feb. 25, 2024; Revision accepted Aug. 8, 2024;
Crosschecked May 12, 2025

accompanies placental development, particularly in the labyrinthine (Lab) layer, a key section of feto–maternal interaction containing blood vessels from both fetal and maternal origins (Xu et al., 2020). Genes such as the C–C motif cytokine ligand 3 (*Ccl3*) and *Ccl4* (Liao et al., 2016; Hu et al., 2020), early growth response 1 (*Egr1*) (Yan et al., 2021), dual-specificity phosphatase 1 (*Dusp1*) (Moncho-Amor et al., 2011), oncostatin M (*Osm*) (Fearon et al., 2006), and serine/threonine kinase family member 1 (*Pim1*) (Chen et al., 2016) have been recognized for their essential roles in regulating angiogenesis. In the mouse placenta, three major cell types involved in angiogenesis include trophoblasts, endothelial cells, and different types of immune cells (monocytes, macrophages, and dendrites) (Kuo et al., 2019; Dunk et al., 2021; Thomas et al., 2021). Numerous changes in genes regulating the angiogenesis signaling pathway have been observed in these cell types, including transforming growth factor-β (*TGF-β*), macrophage migration inhibitory factor (*MIF*), angiopoietin-like protein (*ANGPTL*), and secreted class 3 semaphorins (*SEMA3*) (Wang et al., 2013; Carbone et al., 2018; Abu El-Asrar et al., 2019; Jiao et al., 2021).

In the mouse genome, the glutaminyl-peptide cyclotransferase (*Qpct*) allele is positioned on chromosome 17 (chr17: 79 451 246–79 489 583) and encodes the enzyme glutaminyl-peptide cyclotransferase (Busby et al., 1987). Okae et al. (2012) utilized an embryo transfer strategy to remove maternal contamination and concluded that *Qpct* did not exhibit maternal imprinting. However, embryo transfer and in vitro fertilization showed the potential to alter the imprinting status (McDonald et al., 1998; Doherty et al., 2000; Prissette et al., 2001; Mann et al., 2004). In our previous study, after removing the decidual layer and placental chorionic plate to eliminate maternal contamination, we re-identified *Qpct* as a placenta-specific imprinted gene that was maternally expressed in the embryonic Day 15.5 (E15.5) placenta. (Guo et al., 2015). During early embryogenesis, *Qpct* exhibits broad expression at E9.5–E11.5 and is detectable in the telencephalon, midbrain, and rhombencephalon (Guo et al., 2015). However, the role of *Qpct* in governing placental and embryonic development remains largely unexplored.

Recently, single-cell RNA sequencing (scRNA-seq) has proven to be an effective approach (Liu et al., 2018) for exploring the interior heterogeneity of placental tissues (Pique-Regi et al., 2019). Although scRNA-seq offers significant advantages, it also encounters technical limitations, such as the under-representation of syncytiotrophoblasts in placenta research (Suryawanshi et al., 2018; Vento-Tormo et al., 2018). Single-nucleus RNA sequencing (snRNA-seq) overcomes certain challenges by focusing on gene expression at the nuclear level, making it especially useful for tissues that are challenging to dissociate into individual cells (Ding et al., 2020). The snRNA-seq has been used successfully to identify transcript profiles, cell trajectories, and signaling interactions, and infer cellular functions in studies of the mouse placental labyrinth (Marsh and Blelloch, 2020). An analysis of fresh and frozen tumor samples using scRNA-seq and snRNA-seq revealed that both techniques detected comparable cell types, although snRNA-seq identified fewer immune cells (Slyper et al., 2020). Thus, combining scRNA-seq and snRNA-seq offers a comprehensive approach to study placental development, leveraging the strengths of both techniques to yield in-depth insights into cellular and molecular mechanisms.

In this study, we aim to investigate the regulatory role of the placenta-specific imprinted gene *Qpct* in placental angiogenesis. Using clustered regularly interspaced short palindromic repeats (CRISPR)/CRISPR-associated protein 9 (Cas9)-mediated genome editing, we generated global *Qpct*-knockout mice to examine the impact of gene deletion on vascular development during mid-gestation. By integrating scRNA-seq and snRNA-seq, we comprehensively profile transcriptomic alterations and intercellular communication dynamics within key angiogenesis-related cell populations. This combined approach enables us to elucidate the molecular mechanisms through which *Qpct* orchestrates placental vascular remodeling, thereby providing novel insights into the pathophysiology of angiogenesis-associated placental disorders and identifying potential therapeutic targets.

2 Materials and methods

2.1 Animal maintenance and embryo preparation

Qpct-knockout mice on a C57BL/6J background were generated by the application of CRISPR/Cas9 genome editing technology at the Shanghai Model Organisms Center (China). Two guide RNAs (gRNAs) were designed to delete the genomic DNA that spans

exons 1–5 of the mouse *Qpct* allele. Fertilized eggs were injected with a combination of Cas9 messenger RNA (mRNA) and gRNA, followed by implantation into pseudo-pregnant female mice. The offspring were genotyped by polymerase chain reaction (PCR) to identify the targeted mutations with the gRNA primers listed in Table S1. Successful mating was verified by the detection of a vaginal plug the next morning, which was designated as E0.5. Mice were given unrestricted access to food and water. They were maintained under a standard 12-h light/dark cycle in ventilated cages, housing a maximum of five animals per cage, at a temperature of (23±2) ℃. $Qpct^{-/-}$ and $Qpct^{+/+}$ were obtained by crossing *Qpct* heterozygotes. Four embryonic genotypes were determined by PCR analysis of DNA derived from the amnion with a single 372-bp band with primers P3 and P4 for $Qpct^{+/+}$, a single 1268-bp band with primers P1 and P2 for $Qpct^{-/-}$, and two bands of 1268 bp and 372 bp for $Qpct^{+/-}$ (indicating loss of the paternal allele) and $Qpct^{-/+}$ (indicating loss of the maternal allele) hybrid offspring, respectively.

2.2 Histological analysis of embryos and placentae

At embryonic stages E12.5, E15.5, and E18.5, placentae and embryos of the four genotypes ($Qpct^{+/+}$, $Qpct^{+/-}$, $Qpct^{-/+}$, and $Qpct^{-/-}$) were meticulously separated from surrounding fetal membranes and weighed (n=24 or 25 for each embryonic developmental stage). E15.5 embryos and placentae (the Lab zone upward) of four genotypes (n=6 or 7 for each genotype) were examined using a stereomicroscope model SZX7 from Olympus (Tokyo, Japan). E15.5 placentae of four genotypes (n=6 for each genotype) were preserved using 4% (0.04 g/mL) paraformaldehyde, embedded in paraffin blocks, and sliced into thin sections and subsequently utilized to analyze morphological features with hematoxylin and eosin (H&E) staining. The morphology of placentae was examined using a microscope and the images were evaluated with ImageJ software version 1.8.0 (National Institutes of Health, Bethesda, USA). The pixel size was calculated under the scale bar of the image, and the segmentation and counting features were utilized to measure the area of each placental layer.

2.3 Immunohistochemistry

For the immunohistochemistry analysis, paraffin-embedded E15.5 placentae (n=6 per genotype) were sliced into 5 μm sections, subjected to a dehydration protocol in graded ethanol and xylene, and then rinsed with 1× phosphate-buffered saline (PBS). Antigen retrieval was conducted by incubating the tissue sections in a 10 mmol/L sodium citrate buffer (pH 6.0) at 100 ℃ for 10 min. Sections were pre-treated with 5% (volume fraction) bovine serum albumin (BSA) in PBS for 1 h to prevent non-specific binding, followed by an overnight incubation at 4 ℃ with the designated primary antibodies: anti-Qpct (1:100 (volume ratio, the same below), HPA008406, Sigma, Germany; PA5-76997, Thermo Fisher Scientific, USA), anti-cluster of differentiation 31 (anti-CD31; 1:50, ab222783, Abcam, Cambridge, UK) for endothelial cells, and anti-TOMM20 (1:100, ab186735, Abcam) for mitochondrial staining. After being washed three times with PBS, the sections were incubated for 1 h at 37 ℃ with an Alexa Fluor 488-conjugated anti-rabbit secondary antibody (1:1000, 111545003, Jackson ImmunoResearch, USA). Subsequently, the sections were stained with 4',6-diamidino-2-phenylindole (DAPI; Invitrogen, CA, USA) for 10 min at room temperature. Fluorescence visualization was conducted using a fluorescence microscope (Olympus IX71, Olympus, Japan) under proper exposure settings.

2.4 qRT-PCR

Placentae were harvested from $Qpct^{+/+}$, $Qpct^{+/-}$, $Qpct^{-/+}$, and $Qpct^{-/-}$ mice at E15.5. Total RNA was extracted and complementary DNA (cDNA) was generated using the Superscript™ III RNase H-Reverse Transcriptase Kit (Invitrogen). The quantitative reverse transcription-polymerase chain reaction (qRT-PCR) was conducted with the SYBR Premix Ex Taq™ Kit (TaKaRa, Shiga, Japan) on an ABI PRISM 7500 Real-Time PCR System (Applied Biosystems, CA, USA). Details of the primer sequences are provided in Table S1. The cycle threshold (C_T) values were adjusted relative to β-actin expression. Each experiment was conducted in triplicate for each specimen.

2.5 Tissue dissociation, single-cell preparation, and 10× Genomics RNA-seq of the mouse placentae

Placentae from E15.5 $Qpct^{+/+}$ and $Qpct^{-/-}$ mice were processed using a recently developed cell dissociation protocol and analyzed with 10× Genomics technology (Nelson et al., 2016). In brief, three placental specimens were pooled and gently dissected

using fine scissors and digested in a solution containing Liberase™ (0.325 Wunsch U/mL, Roche, Switzerland), Deoxyribonuclease I (DNase I; 20 Kunitz U/mL, Sigma), and RNase inhibitor (20 U/mL, Thermo Fisher Scientific) in Dulbecco's modified Eagle's medium (DMEM) supplemented with 15% (volume fraction) fetal calf serum (FCS), 10% (volume fraction) National Collection of Type Cultures (NCTC)-109 medium (Gibco, USA), 15 mmol/L *N*-(2-hydroxyethyl)piperazine-*N*'-(2-propanesulfonic acid) (HEPES) buffer, 0.1 mmol/L non-essential amino acids, 2 mmol/L glutamine, and 1% (volume fraction) Hybri-Max Oxaloacetate+Pyruvate+Insulin (OPI) supplement (Sigma). The tissue was incubated for 45 min at 37 °C with continuous shaking for cellular dissociation. The cell suspension was then filtered through a 100-μm mesh filter to remove tissue debris. Ice-cold PBS containing 0.4% (volume fraction) BSA was used to resuspend the filtered cells, which were then processed using the Chromium Single Cell 3' Library & Gel Beads Kit v3 i7 (10× Genomics) for subsequent scRNA-seq procedures.

For snRNA-seq, the nuclei of E15.5 mouse placentae ($Qpct^{+/+}$ and $Qpct^{-/-}$) were isolated according to the previous manuals (Marsh and Blelloch, 2020). Placental tissues were carefully dissected into small fragments (<1 mm) using a razor blade and placed in 2 mL of Nuclei EZ lysis buffer (Sigma, MO, USA). Tissue homogenization was conducted using a Dounce homogenizer, applying ten strokes with both loose and tight pestles (A and B). The homogenized material was then transferred to a 15 mL Falcon tube with an additional 2 mL of Nuclei EZ lysis buffer and incubated on ice for 5 min. The solution was filtered through a 40-μm mesh and centrifuged at 500*g* for 8 min at 4 °C. After the supernatant was discarded, the pellet was resuspended in 2 mL of lysis buffer, kept on ice for another 5 min, and centrifuged again under identical conditions. The nuclei were then filtered through a 35-μm mesh and processed using the Chromium platform with the Single Cell 3' Library & Gel Beads Kit v3 i7 (10× Genomics) for downstream applications.

2.6 Analyses of scRNA-seq and snRNA-seq datasets

The alignment of Illumina sequencing reads to the mouse genome (mm10) was performed using the CellRanger software (version 3.0, 10× Genomics) under default configuration parameters. The Seurat package (version 3.0.0) was employed for the thresholding and analysis of the count matrix. For the scRNA-seq dataset, cells with fewer than 500 detected genes, total read counts outside the range of 1000–110 000, ribosomal protein content above 40% (volume fraction), or mitochondrial gene content above 40% (volume fraction) were excluded. After applying these filtering criteria, 6567 cells from $Qpct^{+/+}$ placentae and 3285 cells from $Qpct^{-/-}$ placentae were retained for subsequent analyses. For the snRNA-seq dataset, nuclei exhibiting fewer than 500 or more than 6000 detectable genes, or those with mitochondrial gene percentage exceeding 5% and ribosomal protein gene percentage over 5% were removed. After applying these filtering criteria, 8880 nuclei from $Qpct^{+/+}$ placentae and 13 577 nuclei from $Qpct^{-/-}$ placentae were retained for subsequent analyses. The ScaleData and NormalizeData functions were applied to scale and normalize the scRNA-seq and snRNA-seq data with default configurations. The FindVariableFeatures function was used to pinpoint the top 2000 genes with the greatest variability, which were subsequently used as the foundation for subsequent analytical processes. Principal component analysis (PCA) was executed with the RunPCA function, and the significance of the principal components was evaluated with the ElbowPlot and DimHeatmap functions. RunUMAP function was used to conduct dimensionality reduction and visualization.

Multiple cell type-specific markers were collected for cell-type identification, including α-smooth muscle actin (*Acta2*), decorin (*Dcn*), and high-temperature requirement factor a3 (*Htra3*) for decidual cells (Singh et al., 2011; Vento-Tormo et al., 2018; Halari et al., 2020); *Cd34*, vascular endothelial growth factor (VEGF) receptor 2 (*Vegfr2*/*Kdr*), and plasmalemma vesicle-associated protein (*Plvap*) for endothelial cells (Strickland et al., 2005; Nelson et al., 2016; Marsh and Blelloch, 2020); connective tissue growth factor protein (*Ccn2*) and Glu/Asp-rich carboxy-terminal domain 1 (*Cited1*) for trophoblasts (Moussad et al., 2002; Xu et al., 2018); cathepsins q (*Ctsq*) and leptin receptor (*Lepr*) for trophoblast giant cells (TGCs) (Outhwaite et al., 2015); prune homolog 2 (*Prune2*) and neural cell adhesion molecule1 (*Ncam1*) for glycogen trophoblast (GlyT) (Dalangood et al., 2020; Marsh and Blelloch, 2020); *Cts3*, *Ctsm*, and prolactin 8a9 (*Prl8a9*) for spongiotrophoblast (SpT) (Bode et al., 2005; Marsh and Blelloch, 2020); transferrin receptor (*Tfrc*) for syncytiotrophoblast (SynT) (Marsh and Blelloch,

2020); trigger receptor expressed in myeloid-like 4 (*Treml4*), eosinophil-associated ribonuclease A family member 2 (*Ear2*), lymphocyte antigen 6 family member C2 (*Ly6c2*), chitinase-like 3 (*Chil3*), and cytochrome b-245, β polypeptide (*Cybb*) for monocytes (Larson et al., 2016; Olsson et al., 2016; Jakubzick et al., 2017; Jaitin et al., 2019; Trzebanski and Jung, 2020); complement C1q subcomponent subunit a (*C1qa*), *C1qb*, *C1qc*, mannose receptor C-type 1 (*Mrc1*), and triggering receptor expressed on myeloid cells 2 (*Trem2*) for macrophages (Farmer et al., 2017; Hou et al., 2021; Picton et al., 2021); *Cd209a*, FMS-like tyrosine kinase 3 (*Flt3*), and kynurenine-3-monooxygenase (*Kmo*) for dentritic cells (Menezes et al., 2016); neoglycoproteins (*Ngp*), cyclic adenosine 3',5'-monophosphate (*Camp*), S100 calcium-binding protein A8 (*S100a8*), *S100a9*, and colony-stimulating factor 3 receptor (*Csf3r*) for neutrophil cells (Hong et al., 2019; Zhang et al., 2019); Granzyme A (*Gzma*) and *Gzmb* for natural killer (NK) cells (Arauzo-Bravo et al., 2020); mast cell protease 8 (*Mcpt8*) and GATA-binding protein 2 (*Gata2*) for basophil cells (Sullivan et al., 2011; Sasaki et al., 2016); *Cd3e*, *Cd4*, and transcription factor 1 gene (*Tcf7*) for T cells (Medaglia et al., 2017; Stoeckius et al., 2017); *Cd79a*, *Cd79b*, and early B cell factor 1 (*Ebf1*) for B cells (Korkolopoulou et al., 1994; Medaglia et al., 2017; Bullerwell et al., 2021). The markers used for cell type identification are detailed in Table S2.

2.7 Differential gene expression of E15.5 *Qpct*$^{+/+}$ and *Qpct*$^{-/-}$ mouse placentae at the single-cell resolution

Differentially expressed genes (DEGs) between E15.5 *Qpct*$^{+/+}$ and *Qpct*$^{-/-}$ placentae were identified via the Seurat FindMarkers function with the Wilcoxon test approach. A cutoff of adjusted $P<0.05$ and absolute $\log_2$(fold change)>0.1 was applied in the analysis. Volcano plots were created using the ggplot2 package for data visualization.

2.8 Pathway enrichment analyses of E15.5 *Qpct*$^{+/+}$ and *Qpct*$^{-/-}$ mouse placentae

Gene set enrichment analysis (GSEA) was conducted to investigate the biological pathways across different cell types (including all cells, endothelial cells, trophoblasts, TGCs, and immune cells) through the R package clusterProfiler (version 3.18.1). Gene sets were sourced from https://bioinf.wehi.edu.au/MSigDB/v7.1. Statistical significance was determined based on a false discovery rate (FDR) of <0.25.

2.9 Gene–gene co-expression network of *Qpct* and related imprinted genes

The scLink method (Li and Li, 2021) was applied to construct sparse co-expression networks of imprinted genes and seven down-regulated genes (delta-like 1 homolog (*Dlk1*), maternally expressed gene 3 (*Meg3*), *Igf2*, paternally expressed gene 10 (*Peg10*), *Peg3*, potassium voltage-gated channel subfamily Q member 1 overlapping transcript 1 (*Kcnq1ot1*), and zinc finger, DBF-type containing 2 (*Zdbf2*)) in *Qpct*$^{-/-}$ placental all cells, immune cells, endothelial cells, and TGCs. The correlation value was calculated by the scLink_cor function, and the network was created by the R package igraph (version 2.0.5).

2.10 Cell–cell communication analysis

The R package CellChat (version 1.1.3) (Jin et al., 2021) was employed to analyze the signaling interactions between various cell types in our single-cell transcriptomic dataset. We generated a CellChat object of *Qpct*$^{+/+}$ and *Qpct*$^{-/-}$ placentae data separately using the createCellChat and computeCommunProbPath functions. The function mergeCellChat was used to merge the objects. The function netAnalysis_signalingRole_heatmap with parameter pattern="all" was used to compare overall signaling of the *Qpct*$^{+/+}$ and *Qpct*$^{-/-}$ datasets. Function subsetCommunication with parameters ligand.logFC=0.1 and thresh=0.05 was used to obtain up-regulated and down-regulated ligand–receptor pairs. Statistical significance was defined as $P<0.05$ and $|\log_2(\text{fold change})|>0.1$.

2.11 Statistical analysis

Data are displayed as mean±standard deviation (SD) and are derived from a minimum of four independent experiments. Statistical evaluation was conducted using *t*-tests, with significance considered at $P<0.05$.

3 Results

3.1 Embryonic and placental overgrowth in *Qpct*-knockout conceptuses

We previously identified *Qpct* as an imprinted gene in the placenta that was expressed from the maternal allele (Guo et al., 2015). To investigate its

role in placental and embryonic development, we generated *Qpct* null (*Qpct*$^{-/-}$), maternal-*Qpct* knockout (*Qpct*$^{-/+}$), and paternal-*Qpct* knockout (*Qpct*$^{+/-}$) mice using the CRISPR/Cas9 platform (Fig. 1a). Our results demonstrated that the size of the embryo and placenta significantly increased in E15.5 *Qpct*$^{-/+}$ and *Qpct*$^{-/-}$ conceptuses, with no change in *Qpct*$^{+/+}$ or *Qpct*$^{+/-}$ (Fig. 1b). Embryonic and placental weights in *Qpct*$^{-/+}$ and *Qpct*$^{-/-}$ mice were higher at each time point (E12.5, E15.5, and E18.5) than those observed in *Qpct*$^{+/+}$ and *Qpct*$^{+/-}$ mice (P<0.05; Figs. 1c and 1d). Compared with that of wild-type controls, the weight of the embryo increased, especially at E15.5 when it increased by 175%, while the placental weight increased by 50% in *Qpct*$^{-/+}$ and *Qpct*$^{-/-}$ mice. Additionally, we detected the expression of *Qpct* in E15.5 and E18.5 embryos and placentae in the four genotypes (Fig. 1e). The expression of *Qpct* decreased to 50% in E15.5 and

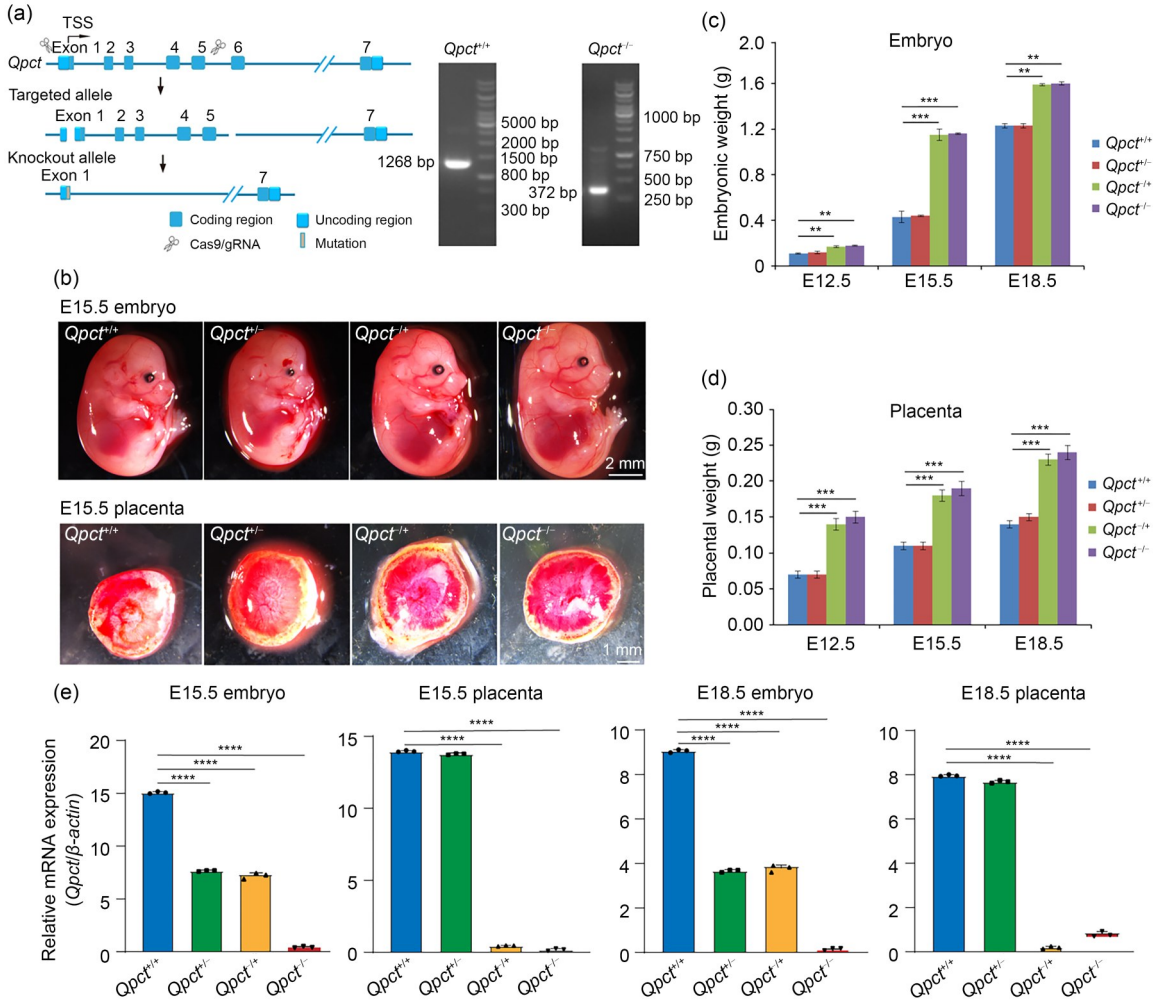

Fig. 1 Generation of glutaminyl-peptide cyclotransferase (*Qpct*)-knockout mice and histological analysis of placentae and embryos in the four genotypes of *Qpct*-knockout mice. (a) Diagrammatic representation of the approach for constructing *Qpct*-knockout mice with clustered regularly interspaced short palindromic repeats (CRISPR)/CRISPR-associated protein 9 (Cas9) technology. TSS: transcription start site; gRNA: guide RNA. (b) Size comparison of *Qpct*$^{+/+}$, *Qpct*$^{+/-}$, *Qpct*$^{-/+}$, and *Qpct*$^{-/-}$ embryos and placentae during the E15.5 developmental stage (n=6 or 7 for each genotype). (c, d) Embryonic (c) and placental (d) weights of four genotypes (*Qpct*$^{+/+}$, *Qpct*$^{+/-}$, *Qpct*$^{-/+}$, and *Qpct*$^{-/-}$) were measured at different embryonic developmental stages (E12.5, E15.5, and E18.5). Data are presented as mean±standard deviation (SD), with sample sizes of n=24 or 25 for each embryonic stage and n=6 or 7 for each genotype. ** P<0.01 and *** P<0.001 denote significant differences in the embryonic and placental weights of *Qpct*$^{-/+}$ or *Qpct*$^{-/-}$ compared to the *Qpct*$^{+/+}$ group at the respective stages (E12.5, E15.5, and E18.5). (e) Messenger RNA (mRNA) expression of *Qpct* in the embryos and placentae of the four genotypes at E15.5 and E18.5. Data are presented as mean±SD, with n=6 for each genotype. Statistical significance is denoted as **** P<0.0001, reflecting notable differences at mRNA expression levels relative to the *Qpct*$^{+/+}$ group.

E18.5 *Qpct*$^{+/-}$ and *Qpct*$^{-/+}$ embryos compared with *Qpct*$^{+/+}$. In the placentae, the expression of *Qpct* in *Qpct*$^{+/-}$ was the same as in *Qpct*$^{+/+}$, while it was nearly absent in *Qpct*$^{-/+}$ and *Qpct*$^{-/-}$. In summary, these results indicate that maternal *Qpct* deficiency may contribute to excessive development of both the embryo and placenta. This aligns with the theory of "parental conflict," where genes expressed from the maternal allele act to regulate and constrain the growth of the conceptus (Fowden et al., 2011).

3.2 Histological analysis of placentae revealing unequal expansion of placental sections in maternal *Qpct*-knockout mice

H&E staining was performed in the four genotypes to examine the impact of maternally expressed *Qpct* on the internal placental anatomy. We found that placentae of *Qpct*$^{-/+}$ and *Qpct*$^{-/-}$ exhibited an abnormal enlargement of the junctional zone (JZ) (Fig. 2a), which was consistent with a previous report showing that maternally expressed imprinted genes such as pleckstrin

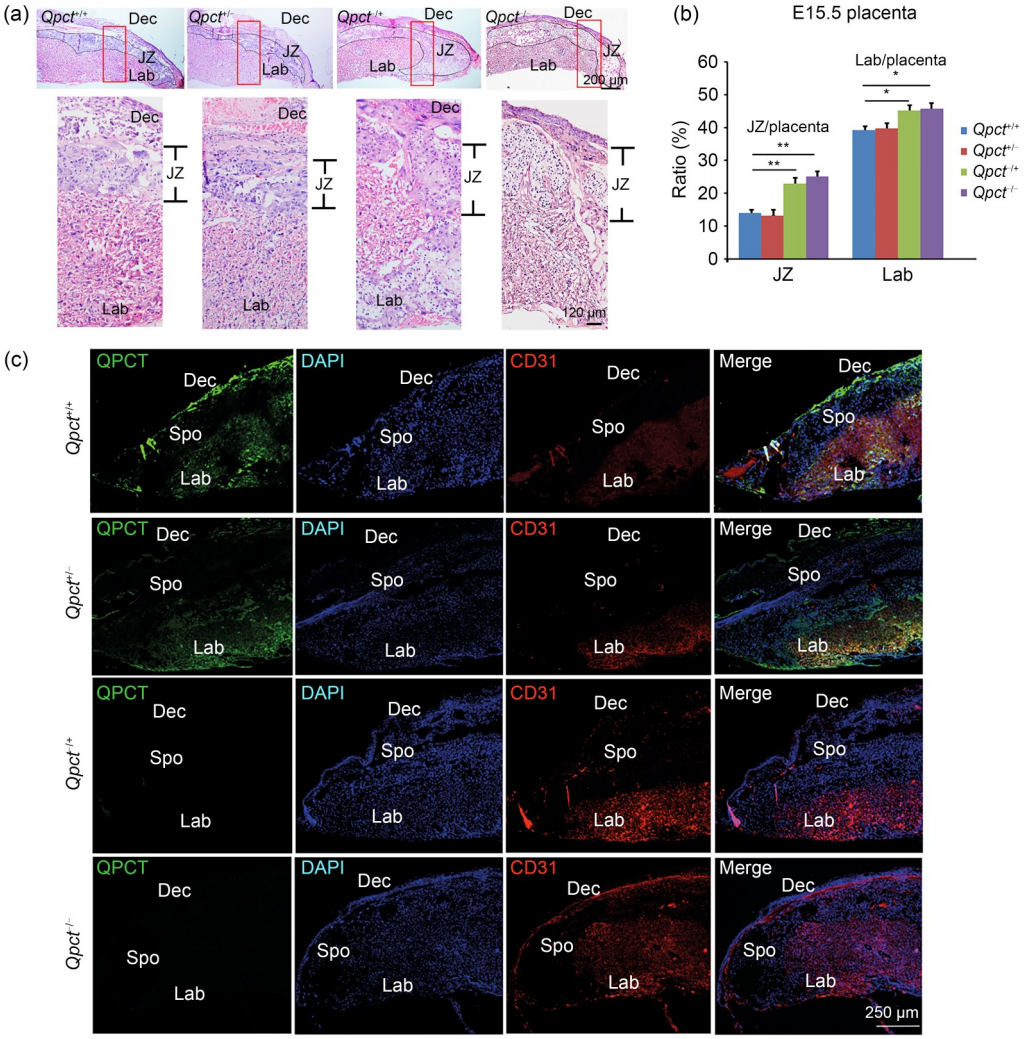

Fig. 2 Histological evaluation of placental abnormalities in glutaminyl-peptide cyclotransferase (*Qpct*)$^{-/+}$ and *Qpct*$^{-/-}$ mice at E15.5. (a) Hematoxylin and eosin (H&E) staining of placentae from the four genotypes. Black lines indicate the decidual (Dec; top), the junctional zone (JZ; middle), and the labyrinthine (Lab; bottom) layers. The upper panels display the enlarged view, while the lower panels present higher-magnification images (*n*=6 per genotype). (b) JZ/placenta and Lab/placenta area ratios relative to total area of the four genotypes (*n*=6). The values are presented as mean± standard deviation (SD). * *P*<0.05 and ** *P*<0.01 for the ratios of JZ/placenta and Lab/placenta of *Qpct*$^{-/+}$ or *Qpct*$^{-/-}$ mice vs. *Qpct*$^{+/+}$ mice at E15.5 (*n*=6 for each genotype). (c) Immunohistochemical assessment of QPCT and cluster of differentiation 31 (CD31) expression in placentae of the four genotypes at E15.5. Spo: spongioblast layer (*n*=6 for each genotype); DAPI: 4',6-diamidino-2-phenylindole.

homology-like domain family A member 2 (*Phlda2*) could enlarge the placenta (Tunster et al., 2016). Moreover, at E15.5, *Qpct*$^{+/+}$ and *Qpct*$^{-/-}$ mice exhibited a significant expansion of both JZ and Lab layer, as indicated by elevated JZ/placenta and Lab/placenta ratios. Specifically, the JZ/placenta ratios were about 70% larger and the Lab/placenta ratios about 18% larger in *Qpct*$^{-/+}$ and *Qpct*$^{-/-}$ than in *Qpct*$^{+/+}$ (P<0.01 and P< 0.05; Fig. 2b). Meanwhile, in the *Qpct*$^{+/+}$ placenta, the ratios of JZ and Lab layers were 14.2% and 39.3%, respectively, with a decidual ratio of 46.5%. In the *Qpct*$^{-/+}$ and *Qpct*$^{-/-}$ placentae, the ratios of JZ and Lab layers were about 23%–25% and 45%–46%, respectively, with the decidual ratio around 30% (Fig. 2b). The smaller decidual ratio indicated the impact of the maternal genotype of the imprinted gene *Qpct*. The immune-cytochemistry results demonstrated the presence of QPCT signal in the decidual and Lab layers in *Qpct*$^{+/+}$ and *Qpct*$^{+/-}$ mice at E15.5, with weaker expression observed in the JZ (Fig. 2c). As expected in knockout animals, the QPCT signal was very weak to non-existent in the decidual and Lab layers in *Qpct*$^{-/+}$ and *Qpct*$^{-/-}$ mice. Collectively, the findings indicate that maternal *Qpct* deficiency leads to anatomical changes in the placenta, specifically the expansion of the JZ and Lab layers, which in turn impacts overall placental function.

3.3 Single-cell analysis revealing transcriptional and proportional differences between *Qpct*$^{+/+}$ and *Qpct*$^{-/-}$ E15.5 placentae

To gain more precise insights into the cellular transcriptome changes resulting from the knockout of the imprinted gene *Qpct*, we carried out both scRNA-seq and snRNA-seq of placental cells from E15.5 *Qpct*$^{+/+}$ and *Qpct*$^{-/-}$ mouse placentae (Fig. 3a). A total of 32 309 distinct cellular transcriptomic profiles were grouped and analyzed using pooled samples from mouse placentae of each genotype: 8880 cells from *Qpct*$^{+/+}$ placentae and 13 577 cells from *Qpct*$^{-/-}$ placentae via snRNA-seq, and 6567 cells from *Qpct*$^{+/+}$ placentae and 3285 cells from *Qpct*$^{-/-}$ placentae via scRNA-seq (Figs. 3c and 3e). Uniform manifold approximation and projection (UMAP) clustering analysis identified 13 cell clusters (snRNA-seq) and 20 cell clusters (scRNA-seq) based on the representative gene markers (Figs. 3b and 3d).

Careful comparison of the snRNA-seq and scRNA-seq datasets revealed that snRNA-seq captured a higher proportion of cell types, such as sinusoidal trophoblast giant cell (S-TGC), SpT, and SynT, while scRNA-seq identified more immune-related cell types (Fig. 3f). This difference arises because SynT cells are multinucleated, making them unsuitable for the

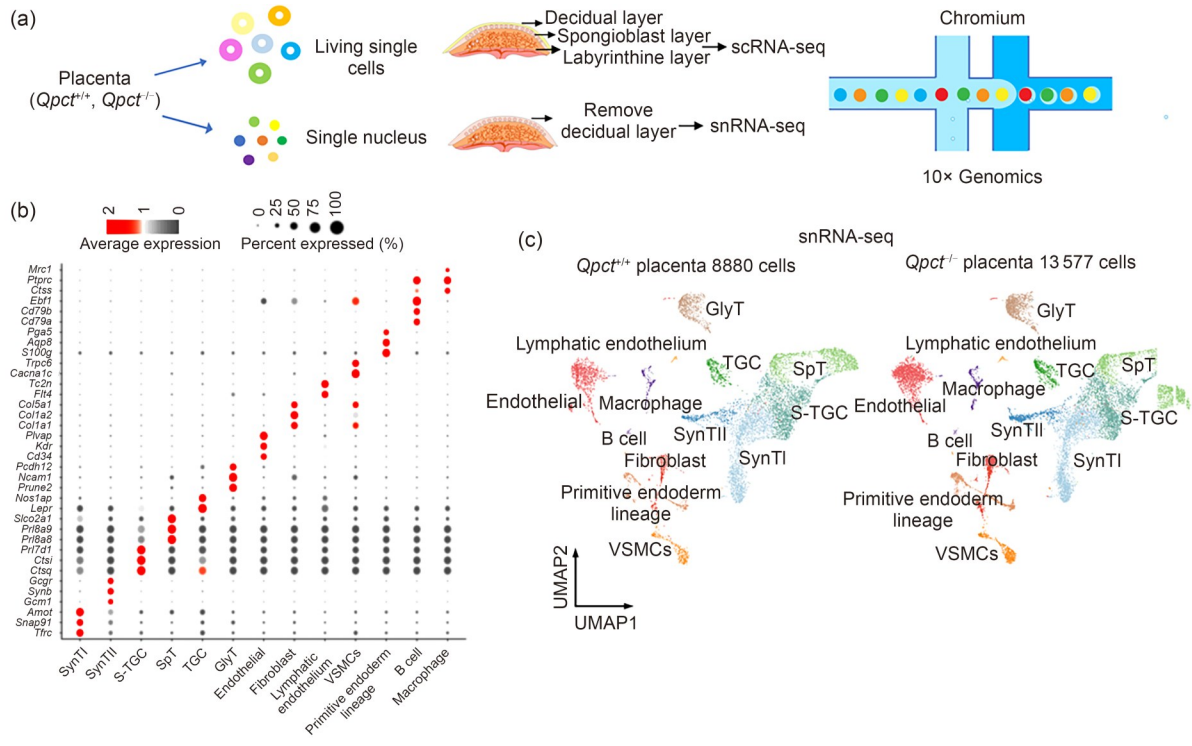

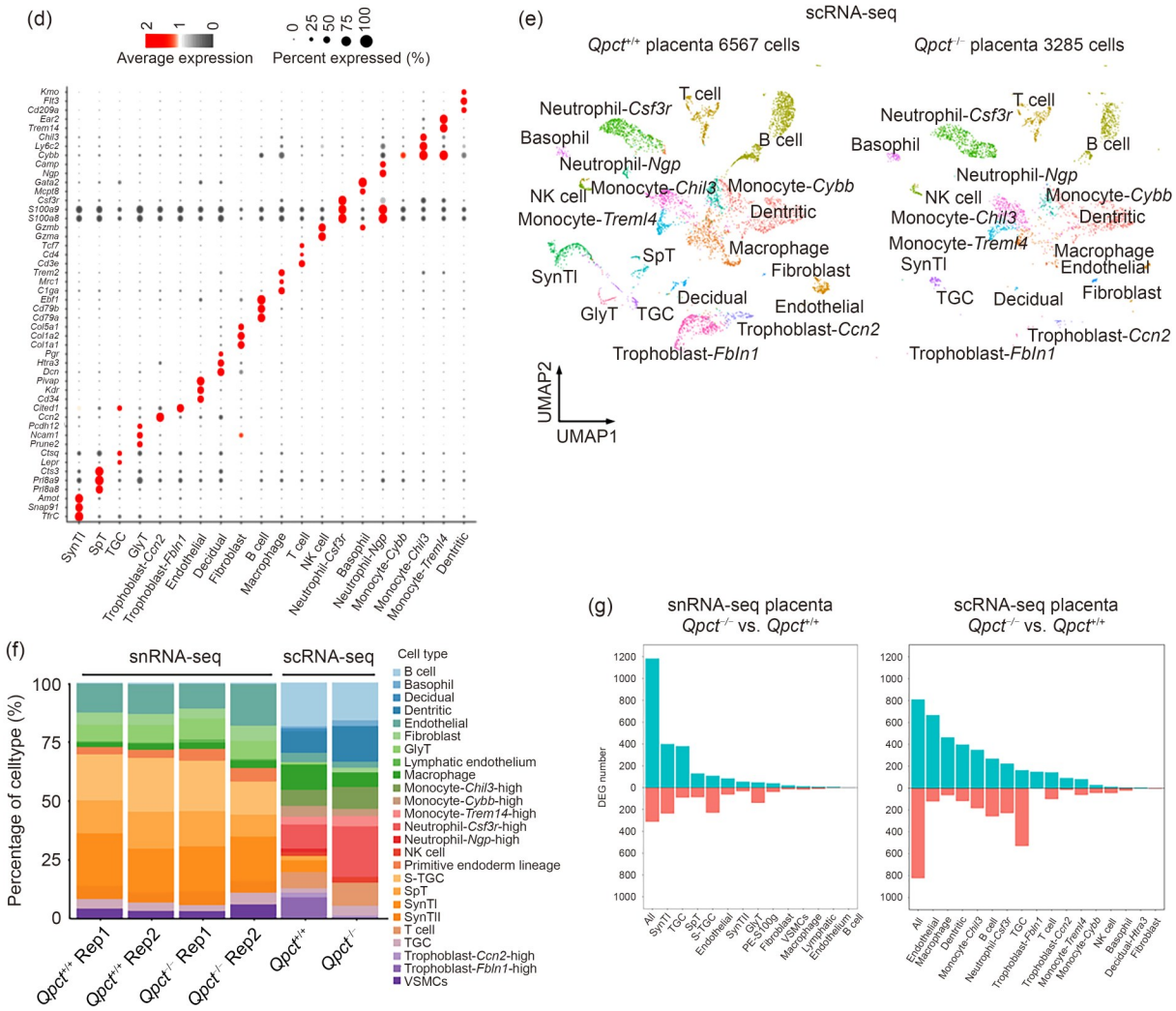

Fig. 3 Single-cell RNA sequencing (scRNA-seq) and single-nucleus RNA sequencing (snRNA-seq) analysis of placental cell types in E15.5 glutaminyl-peptide cyclotransferase (*Qpct*)$^{+/+}$ and *Qpct*$^{-/-}$ mice. (a) Schematic diagram of the snRNA-seq and scRNA-seq experiments in E15.5 *Qpct*$^{+/+}$ and *Qpct*$^{-/-}$ placentae. (b) Dot plot of the expression of marker genes in the snRNA-seq of E15.5 *Qpct*$^{+/+}$ and *Qpct*$^{-/-}$ mouse placentae. (c) Uniform manifold approximation and projection (UMAP) plots of the 13 cell types in the snRNA-seq of E15.5 *Qpct*$^{+/+}$ and *Qpct*$^{-/-}$ placentae. Cells are color-coded by type and labeled adjacent to their respective clusters. (d) Dot plot of the expression of marker genes in the scRNA-seq of E15.5 *Qpct*$^{+/+}$ and *Qpct*$^{-/-}$ mouse placentae. (e) UMAP plots of the 20 cell types in the scRNA-seq of E15.5 *Qpct*$^{+/+}$ and *Qpct*$^{-/-}$ placentae. Cells are color-coded by type and labeled adjacent to their respective clusters. (f) Bar plot of the cell-type proportions in snRNA-seq and scRNA-seq of E15.5 *Qpct*$^{+/+}$ and *Qpct*$^{-/-}$ placentae. (g) Bar plots of differentially expressed gene (DEG) numbers in various cell types in the snRNA-seq and scRNA-seq of E15.5 placentae (*Qpct*$^{-/-}$ vs. *Qpct*$^{+/+}$). The red histogram represents the down-regulated DEG numbers in *Qpct*$^{-/-}$, the blue histogram represents the up-regulated DEG numbers in *Qpct*$^{-/-}$. VSMCs: vascular smooth muscle cells.

typical dissociation and isolation approach (Marsh and Blelloch, 2020). Previous studies have shown that snRNA-seq captures fewer immune cells compared to scRNA-seq from the same tissue (Slyper et al., 2020). Nonetheless, the proportions of various cell types remained relatively stable in placental snRNA-seq samples (Fig. 3f). Using scRNA-seq on *Qpct*$^{+/+}$ and *Qpct*$^{-/-}$ E15.5 placentae, a reduction in the abundance of trophoblast and SynT cells was observed, while inflammatory effector cells (including basophils, dendritic cells, monocyte-*Chil3*-high, neutrophil-*Csf3r*-high, and T cells) exhibited an obvious increase. In contrast, the analysis of the snRNA-seq dataset verified that the SynT cell proportion stayed constant. However, owing to the limitations of snRNA-seq, fewer immune cell types, such as basophils, dendritic cells,

monocyte-*Chil3*-high, neutrophil-*Csf3r*-high, and T cells, were observed, making it difficult to assess their proportions accurately (Fig. 3f). In the snRNA-seq analysis of *Qpct*$^{-/-}$ compared with *Qpct*$^{+/+}$ placentae, the majority of DEGs were identified in cell types including SynTI, SynTII, TGC, SpT, and S-TGC. In contrast, the scRNA-seq analysis revealed that DEGs were concentrated mainly in B cells, dendritic cells, endothelial cells, macrophages, monocytes, neutrophils, and TGCs (Fig. 3g). Additionally, we have summarized the cell proportions in both scRNA-seq and snRNA-seq datasets in Table S2. In conclusion, these results imply that the abnormalities of placentae resulting from *Qpct* deficiency were related mostly to immune cells, SynT, SpT, and TGC.

3.4 Promotion of placental angiogenesis by *Qpct* deficiency

To gain deeper insight into the physiological role of *Qpct* in placental development, we examined the DEGs in *Qpct*$^{-/-}$ placentae relative to their *Qpct*$^{+/+}$ counterparts. A detailed list of DEGs is provided in Table S2. Among them, we identified ten genes associated with angiogenesis (*Ccl3*, *Ccl4*, *Egr1*, *Dusp1*, brain acid-soluble protein 1 (*Basp1*), angiopoietin-1 (*Angpt1*), histone deacetylase 9 (*Hdac9*), *Grb10*, phosphodiesterase 4d (*Pde4d*), and latent transforming growth factor β-binding protein 1 (*Ltbp1*)) that were significantly up-regulated in *Qpct*$^{-/-}$ placentae compared to *Qpct*$^{+/+}$ placentae, as revealed by both scRNA-seq and snRNA-seq datasets from E15.5 placentae (adjusted $P<0.05$; Figs. 4a and 4b). This finding was further validated using qRT-PCR ($P<0.01$; Fig. 4c). Additionally, we assessed the number of placental vessels in four genotypes of *Qpct*-knockout mice using immunofluorescence staining with QPCT and CD31 antibodies, which are typical markers of blood vessel endothelial cells. Immunofluorescence staining indicated an increased number of blood vessels in E15.5 *Qpct*$^{-/+}$ and *Qpct*$^{-/-}$ placentae (Figs. 4d and 4e). Furthermore, we analyzed the expression changes of these angiogenesis-related genes across major cell types. Our scRNA-seq dataset indicated that genes, such as *Basp1*, *Ccl3*, *Ccl4*, *Dusp1*, *Egr1*, *Osm*, and *Pim1*, were expressed mainly in immune cells, including neutrophils, basophils, macrophages, and monocytes (Fig. 4f). Owing to methodological limitations of snRNA-seq for identifying immune cell types (Slyper et al., 2020), we were unable to capture a comprehensive range of immune cells such as neutrophils, basophils, and monocytes. Nonetheless, the snRNA-seq dataset provided extensive profiling of cell types such as SynT, GlyT, and TGC. We observed that other angiogenesis-related genes (*Angpt1*, *Grb10*, *Hdac9*, *Ltbp1*, and *Pde4d*) were up-regulated in SynTI, SynTII, S-TGC, TGC, and GlyT cells (Fig. 4f). Additionally, both scRNA-seq and snRNA-seq found that imprinted genes (including *Apoe*, *Dlk1*, *Igf2*, *Meg3*, *Gnas*, *H19*, *Peg10*, and *Slc38a*) were predominantly down-regulated in endothelial cells, trophoblasts, SynTI, SynTII, SpT, S-TGC, and TGC (Fig. 4f). In summary, these findings suggest that maternal *Qpct* deficiency enhances angiogenesis, likely through the up-regulation of placental expression of angiogenesis-promoting genes, including *Ccl3*, *Ccl4*, *Egr1*, *Dusp1*, *Basp1*, *Angpt1*, *Hdac9*, *Grb10*, *Pde4d*, and *Ltbp1*.

3.5 Cell type-specific reduction of imprinted gene expression in E15.5 mouse *Qpct*$^{-/-}$ placentae

We identified a total of seven known placenta-imprinted genes that were down-regulated in *Qpct*$^{-/-}$ placentae compared with *Qpct*$^{+/+}$ placentae, including *Peg3*, *Igf2*, *Meg3*, *Peg10*, *Kcnq1ot1*, *Zdbf2*, and *Dlk1* ($P<0.05$; Figs. 4a and 4b). qRT-PCR analysis validated the down-regulation of *Peg3*, *Meg3*, and *Peg10* in *Qpct*$^{-/-}$ placentae ($P<0.001$ and $P<0.01$; Fig. 5a). Single-cell sequencing data revealed that *Qpct* was broadly expressed across all cell types in *Qpct*$^{+/+}$ placenta. In *Qpct*$^{-/-}$ background, *Qpct* expression was observed only in the immune cell groups (monocytes, dendritic cells, and macrophages), decidual cells, T and B cells, trophoblasts, and endothelial cells (Figs. 5b and 5e). Gene expression and proportional analysis of *Qpct*$^{+/+}$ and *Qpct*$^{-/-}$ placentae suggested that *Peg3* mRNA expression dramatically decreased in the immune cell groups (monocytes, dendritic cells, and macrophages), B cells, and trophoblasts (Figs. 5c and 5f). Interaction network analysis revealed that the strength of imprinted gene interactions was attenuated in *Qpct*$^{-/-}$ placental immune and endothelial cells (Fig. 5d). In conclusion, our results demonstrated that the loss of maternal *Qpct* expression exhibited a substantial impact on the modulation of other imprinted genes, with a cell-type-specific effect. It is plausible that *Qpct* could interact with these down-regulated imprinted genes to regulate embryonic and placental development by targeting immune and

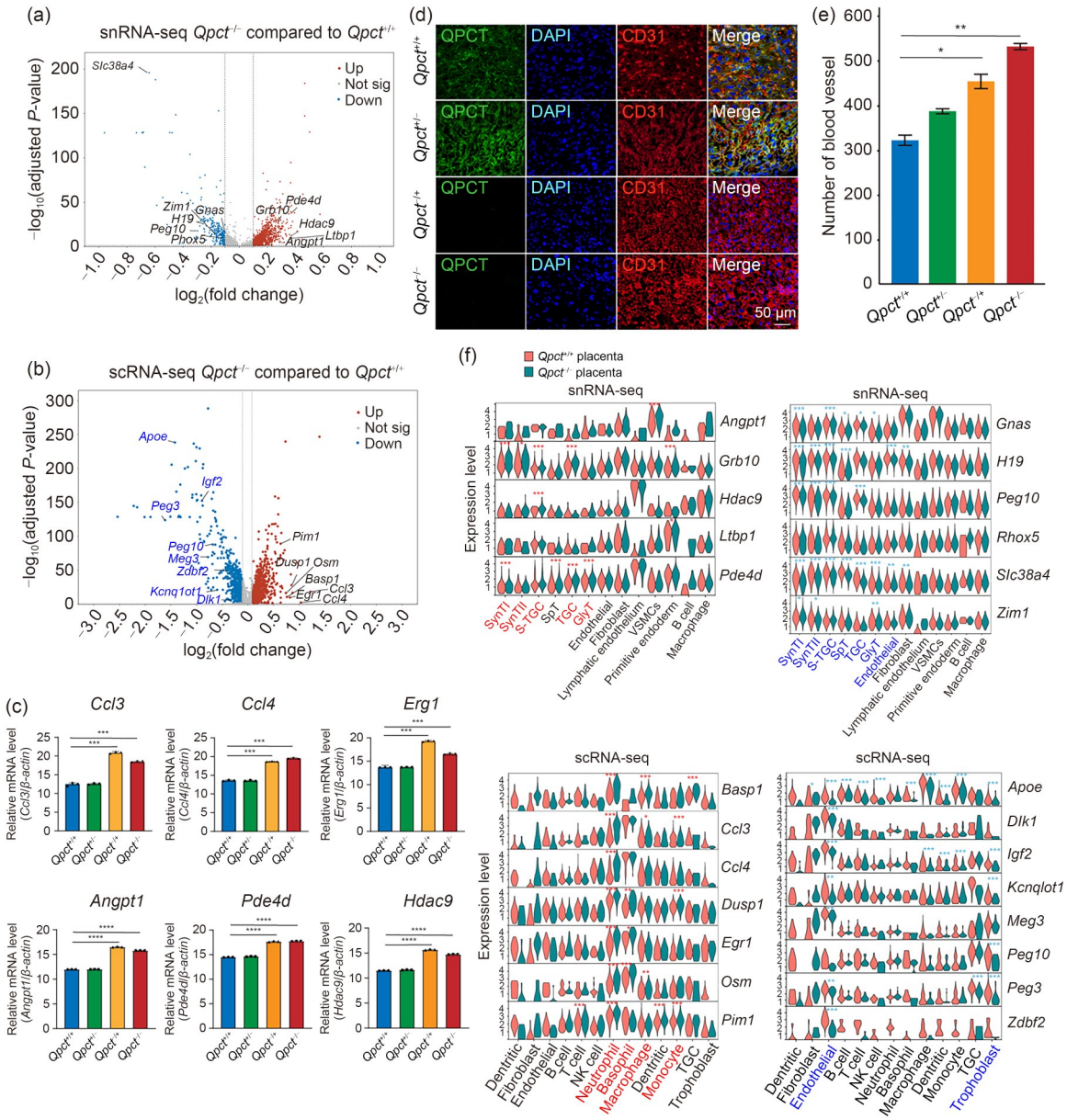

Fig. 4 Glutaminyl-peptide cyclotransferase (*Qpct*) deficiency-induced angiogenesis in the mouse placenta. (a) Volcano plot of differentially expressed imprinted and angiogenesis genes in E15.5 *Qpct*$^{+/+}$ and *Qpct*$^{-/-}$ mouse placentae in single-nucleus RNA sequencing (snRNA-seq) data. The down-regulated (blue) and up-regulated (magenta) genes are marked with gene names in the E15.5 mouse placentae (*Qpct*$^{+/+}$ vs. *Qpct*$^{-/-}$). (b) Volcano plot of differentially expressed imprinted and angiogenesis genes in E15.5 *Qpct*$^{+/+}$ and *Qpct*$^{-/-}$ mouse placentae in single-cell RNA-sequencing (scRNA-seq) data. (c) Messenger RNA (mRNA) expression of the six angiogenic factors (chemokines (*Ccl3* and *Ccl4*), squalene epoxidase (*Erg1*), angiopoietin-1 (*Angpt1*), phosphodiesterase 4d (*Pde4d*), and histone deacetylase 9 (*Hdac9*)) in the placentae of the four genotypes at E15.5. The values are reported as mean±standard deviation (SD), n=6. *** P<0.001, **** P<0.0001. (d) Immunohistochemical evaluation of blood vessels in the decidual and labyrinthine layers of placentas from the four genotypes at E15.5. Placental sections (5 μm thick) were collected at E15.5 and subjected to fluorescent staining using QPCT-antibody, anti-cluster of differentiation 31 (anti-CD31) antibody, and 4',6-diamidino-2-phenylindole (DAPI) (n=6 for each genotype), representing magnified views of the decidual and labyrinth layers in the placental tissue. (e) Quantification of the number of blood vessels within an area of 61 600 μm^2 across the four genotypes at E15.5. Data are expressed as mean±standard deviation (SD). * P<0.05 and ** P<0.01 (n=3 for each genotype). (f) Violin plots illustrating the expression levels of differentially expressed angiogenesis-promoting genes and imprinted genes across various cell types in *Qpct*$^{+/+}$ and *Qpct*$^{-/-}$ placentae, as determined by snRNA-seq and scRNA-seq. Statistical significance is denoted as * P<0.05, ** P<0.01, and *** P<0.001, reflecting differences in gene expression levels between the *Qpct*$^{+/+}$ and *Qpct*$^{-/-}$ groups across each cell type. Not Sig: not significant.

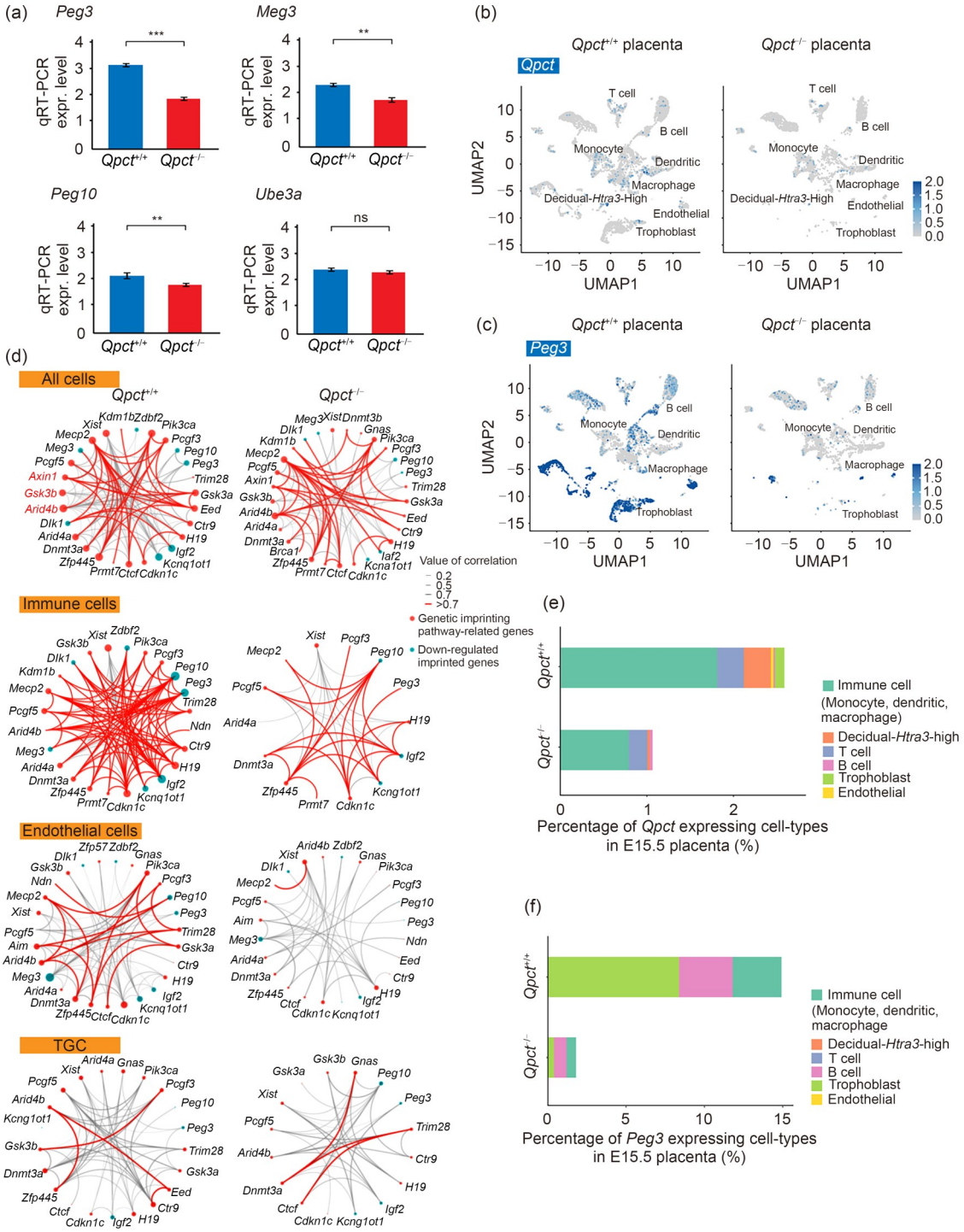

Fig. 5 Analyses of differentially expressed genes in E15.5 glutaminyl-peptide cyclotransferase (*Qpct*)$^{+/+}$ and *Qpct*$^{-/-}$ mouse placentae. (a) Quantitative reverse transcription polymerase chain reaction (qRT-PCR) of differentially expressed imprinted genes in E15.5 mouse placentae (*Qpct*$^{+/+}$ vs. *Qpct*$^{-/-}$). The values are presented as mean±standard deviation (SD), n=6. ** P<0.01, *** P<0.001, and ns (not significant), P>0.05. (b, c) Uniform manifold approximation and projection (UMAP) visualizations depicting the expression levels of *Qpct* (b) and paternally expressed gene 3 (*Peg3*) (c) in E15.5 mouse *Qpct*$^{+/+}$ and *Qpct*$^{-/-}$ placentae. (d) Interaction network diagram of imprinted genes in *Qpct*$^{+/+}$ and *Qpct*$^{-/-}$ placentae (all cells, immune cells, endothelial cells, and trophoblast giant cells (TGCs)). Red line, absolute correlation value >0.7; grey line, absolute correlation value ⩽0.7. Line width represents the strength of the interaction; the node size indicates the number of interactions. (e, f) Bar plots of the ratios of *Qpct*- (e) and *Peg3*-expressing (f) cell types in E15.5 mouse *Qpct*$^{+/+}$ and *Qpct*$^{-/-}$ placentae.

endothelial cells. Taken together, these results suggest that *Qpct* can influence the expression of imprinted genes. Most of the down-regulated imprinted genes were paternally expressed.

3.6 Increase in cell-type-specific communication in promoting angiogenesis signaling pathway in E15.5 mouse *Qpct*$^{-/-}$ placentae

To investigate the functional changes associated with DEGs between *Qpct*$^{-/-}$ and *Qpct*$^{+/+}$ mouse placentae, functional enrichment analysis was performed for these genes in different cell types. We discovered that up-regulated genes in *Qpct*$^{-/-}$ placentae were enriched in protein clusters targeting angiogenesis and vascular development (endothelial cells, trophoblasts, and immune cells), including coronary vasculature development, cardiac conduction system development, vasculogenesis involved in coronary vascular morphogenesis, angiogenesis, and negative regulation of blood coagulation (Fig. 6a). In the cell–cell communication networks promoting the angiogenesis signaling pathway, enhanced communication occurred among endothelia–monocyte and endothelia–macrophage (Fig. 6b); decidual cells–monocyte, decidual cells–macrophage, decidual–dendritic cells, TGC–monocyte, TGC–macrophage, and TGC–dendritic cells (Fig. 6c); endothelial–decidual cells, decidual cells–monocyte, and decidual–dendritic cells (Fig. 6d); and endothelia–macrophage and endothelial–endothelial cells (Fig. 6e). Based on these cell–cell communication changes promoting the angiogenesis signaling pathway, major genes promoting angiogenesis leucine-rich α2 glycoprotein 1 (*Lrg1*), *TGF-β*, *VEGF*, angiopoietin-like 4 (*ANGPTL4*), *MIF*, monocyte chemotactic protein 1 (*MCP1*), interleukin 6 (*IL6*), and *IL8* related to these signaling pathways were up-regulated in *Qpct*$^{-/+}$ and *Qpct*$^{-/-}$ placentae compared with *Qpct*$^{+/-}$ and *Qpct*$^{+/+}$ placentae (Fig. 6f).

In addition, through functional enrichment analysis of the DEGs in different cell types, we also discovered that up-regulated genes in *Qpct*$^{-/-}$ placentae were enriched for protein targeting the mitochondrion (endothelial cells), electron transport chain, oxidative phosphorylation, adenosine triphosphate (ATP) metabolic process, and mitochondrial respiratory chain complex I assembly (TGCs; Fig. 6a). Based on these findings, we further examined the changes in mitochondrial metabolism in *Qpct*$^{-/-}$ placentae (Fig. S1a). Immunofluorescence assays were performed with TOMM20 antibody in the four genotypes of placentae to monitor the changes in mitochondrial distribution. Immunohistochemical results revealed that the mitochondria were distributed mainly in the decidual and Lab layers of placentae in *Qpct*$^{-/+}$ and *Qpct*$^{-/-}$ mice (Fig. S1a). In contrast, they were distributed throughout the whole placentae in *Qpct*$^{+/+}$ and *Qpct*$^{+/-}$ mice (Fig. S1a). The lower cellularity in the *Qpct*$^{-/-}$and *Qpct*$^{-/+}$ placentae spongiotrophoblast layer was reflected by lower mitochondrial density. The expression of mitofusion 1 (*Mfn1*) and mitochondrial transcription factor A (*Tfam*) was examined in the four genotypes of placentae using qRT-PCR, and we noted a marked elevation in both genes in *Qpct*$^{-/+}$ and *Qpct*$^{-/-}$ placentae compared with *Qpct*$^{+/+}$ and *Qpct*$^{+/-}$ mice (P<0.01; Figs. S1b and S1c). These results indicate that *Qpct* may regulate the energy transfer in the placenta by affecting mitochondrial metabolism.

3.7 Identification of specific ligand-receptor pairs promoting angiogenesis in decidual, endothelial, and macrophage cells in E15.5 mouse *Qpct*$^{-/-}$ placentae

To clarify the regulatory mechanism by which specific cell types promote angiogenesis, we compared *Qpct*$^{-/-}$ with *Qpct*$^{+/+}$ placental cells and identified up-regulated ligand–receptor interactions. Cell–cell communication analysis revealed consistently elevated ligand–receptor pairs across multiple cell types (Figs. 7a–7c). Notably, *Mif*–atypical chemokine receptor subtype 3 (*Ackr3*) and *Mif*–(*Cd74*+C-X-C chemokine receptor 4 (*Cxcr4*)) were commonly up-regulated in Acta2^{+} decidual cells, endothelial cells, and macrophages. In contrast, *VEGFβ–VEGFR* and midkine (*Mdk*)–lipoprotein-related receptor 1 (*Lrp1*) were specific to decidual cells; galectin-9 (*Lgals9*)–*Cd44* was shared between endothelial cells and macrophages; and *Ccl3/4–Ccr5* was enriched in macrophages. Consistent with these results, qRT-PCR confirmed the up-regulation of several pro-angiogenic ligand–receptor pairs, including *VEGFβ–VEGFR1*, *Mif–Cd74*, *Mif–Cxcr4*, *Mif–Cd44*, *Mif–Ackr3*, *Mdk–Lrp1*, *Lgals9–Cd45*, *Ccl7–Ccr2*, *Ccl3–Ccr5* and *Ccl4–Ccr5*, in *Qpct*$^{-/+}$ and *Qpct*$^{-/-}$ placentae (Figs. 7d–7h).

4 Discussion

In recent decades, numerous imprinted genes have been identified from high-throughput sequencing

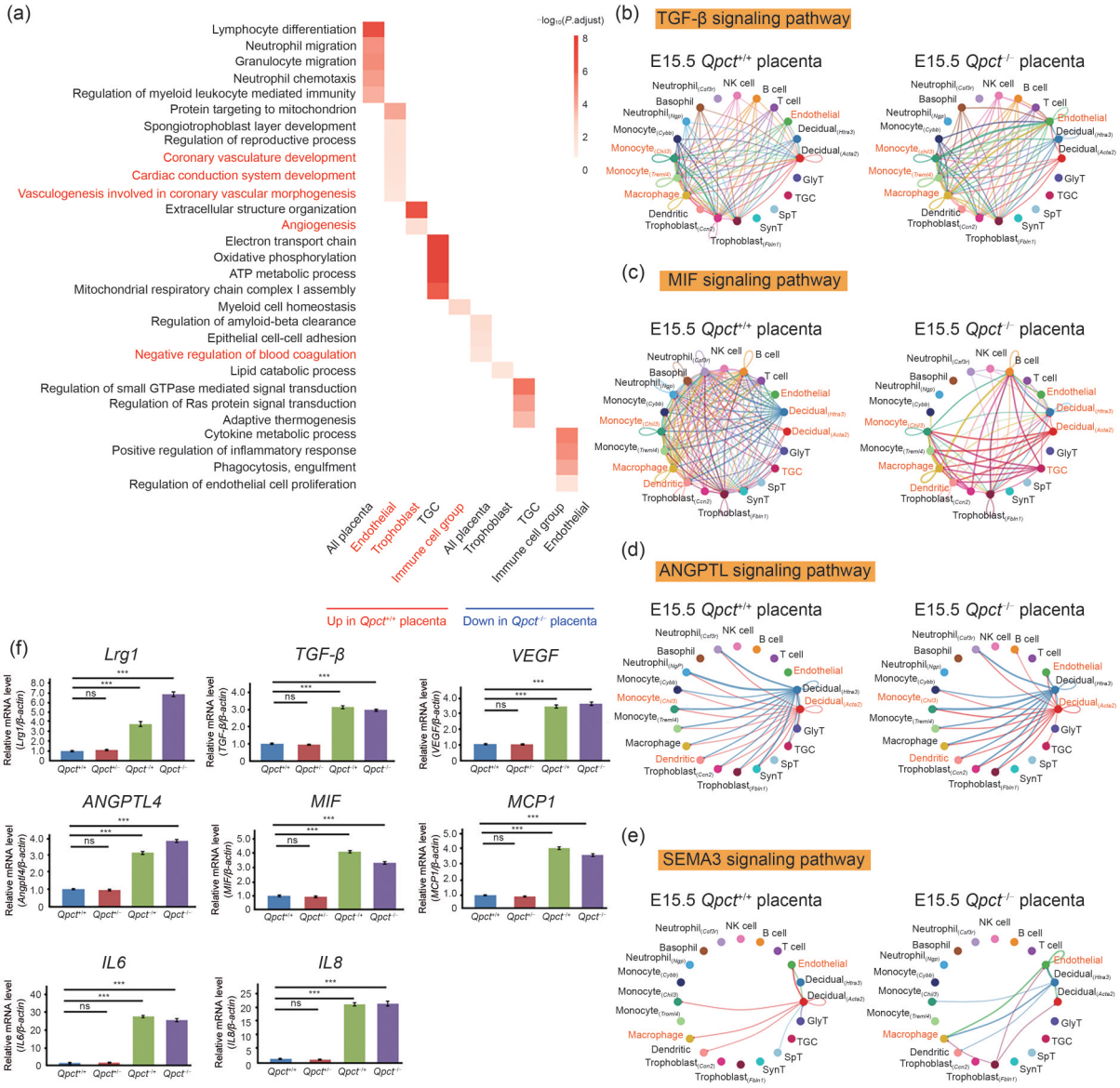

Fig. 6 Analyses of function enrichment and promotion of the angiogenesis signaling pathway in E15.5 glutaminyl-peptide cyclotransferase (*Qpct*)$^{+/+}$ and *Qpct*$^{-/-}$ mouse placentae. (a) The Gene Set Enrichment Analysis (GSEA) of all placentae, endothelial cells, trophoblasts, trophoblast giant cells (TGCs), and immune cells. (b–e) Network plots showing the changes of cell communication of transforming growth factor-β (TGF-β) (b), macrophage migration inhibitory factor (MIF) (c), angiopoietin-like protein (ANGPTL) (d), and secreted class 3 semaphorins (SEMA3) (e) signaling pathways in E15.5 *Qpct*$^{+/+}$ and *Qpct*$^{-/-}$ mouse placentae. The line thickness corresponds to the strength of the interaction, with thicker lines indicating stronger interactions. The nodes of various colors indicate different cell types in E15.5 *Qpct*$^{+/+}$ and *Qpct*$^{-/-}$ placentae. (f) Quantitative reverse transcription polymerase chain reaction (qRT-PCT) of promoting angiogenesis genes in placentae of the four genotypes at E15.5. The values are presented as the mean±standard deviation (SD), n=6. *** P< 0.001 and ns (not significant), P>0.05.

platforms. A comprehensive functional exploration of imprinted genes has elucidated the vital roles of imprinting for the survival of neonates, fetal growth, angiogenesis, cell apoptosis, and regulation of metabolic homeostasis (Miozzo et al., 2001; Peters, 2014; Torres et al., 2017).

Placental development and angiogenesis are vital to embryo development during pregnancy. Angiogenesis involves multiple genes, including *Ccl3*, *Ccl4*, *Egr1*, *Dusp1*, and *Pim1*. Single-cell sequencing and subsequent validation by qRT-PCR revealed increased expression of five angiogenesis-promoting genes in

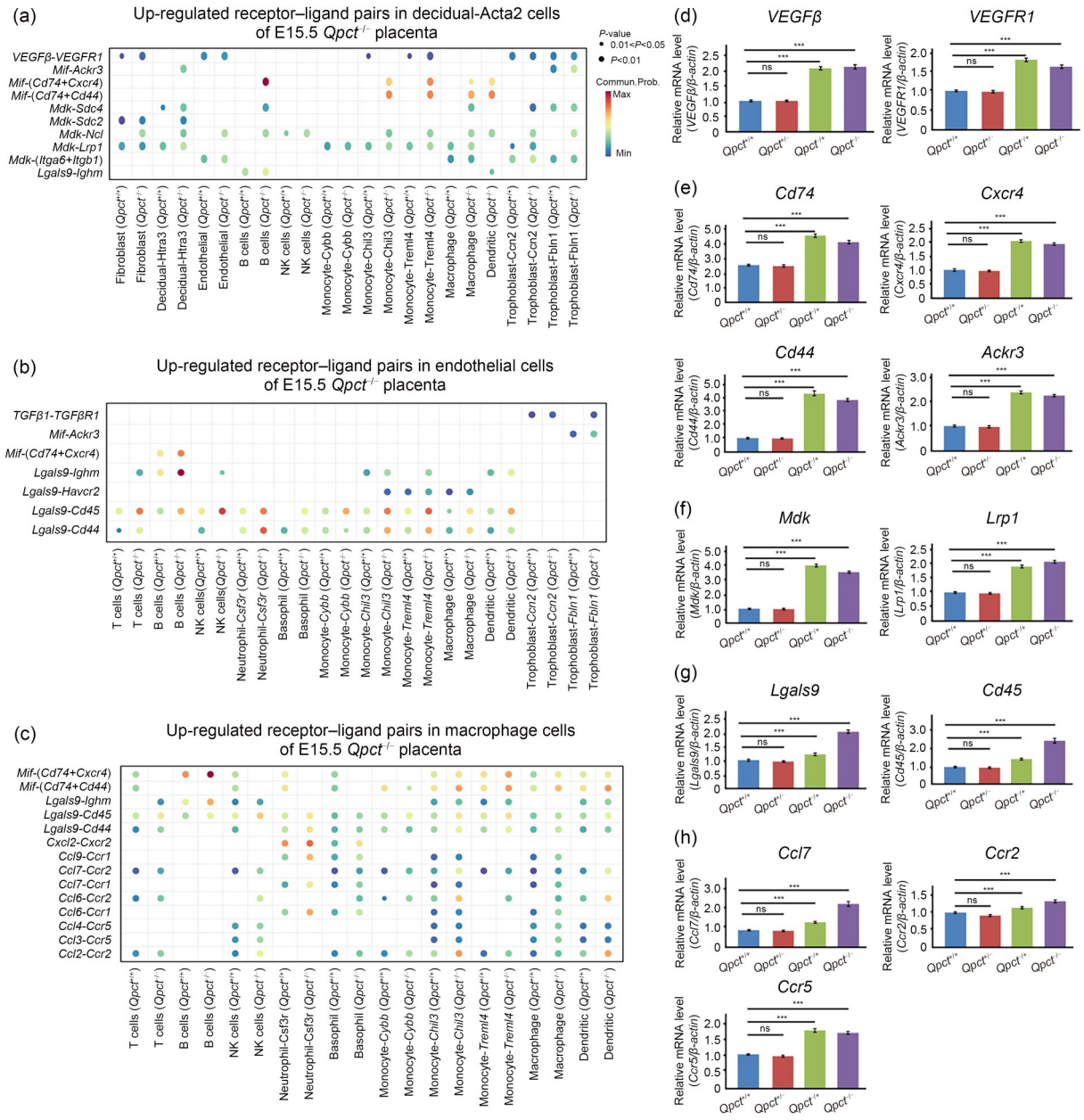

Fig. 7 Identification of up-regulated ligand–receptor pairs in decidual, endothelial, and macrophage cells in E15.5 glutaminyl-peptide cyclotransferase (*Qpct*)$^{-/-}$ placentae. (a–c) Cell communication analysis showed the up-regulated interaction ligand-receptor pairs in decidual, endothelial, and macrophage cells between E15.5 *Qpct*$^{+/+}$ and *Qpct*$^{-/-}$ placentae, * *P*<0.05 and |log$_2$(fold change)|>0.1 were considered significant. (d–h) Quantitative reverse transcription-polymerase chain reaction (qRT-PCR) analysis of ligand-receptor pairs involved in angiogenesis across the four different genotypes of placentas at E15.5. Data are expressed as mean±standard deviation (SD), *n*=6. *** *P*<0.001 and ns (not significant), *P*>0.05.

the placentae of *Qpct*$^{-/+}$ and *Qpct*$^{-/-}$ mice, indicating a possible inhibitory effect of *Qpct* on angiogenesis (Figs. 4a–4e). A previous study demonstrated that placenta-specific imprinted genes were closely linked to the vascularization of the Lab zone and the development of the spongioblast layer (Tunster et al., 2011). These observations align with our findings, which demonstrate a disproportionate expansion of the JZ and Lab layers, along with an increased number of blood vessels and elevated expression of five angiogenesis-promoting genes in *Qpct*$^{-/-}$ and *Qpct*$^{-/+}$ placentae compared with those in *Qpct*$^{+/+}$ and *Qpct*$^{+/-}$ placentae. In the future, standard ex vivo angiogenesis assays will be carried out to explore the important role of *Qpct* in

angiogenesis. Furthermore, immune cells are crucial in facilitating angiogenesis (Jaipersad et al., 2014; Li et al., 2017; McCoy et al., 2021). The proportion of immune cell clusters (T cell, neutrophil, basophil, monocyte, and dendritic cells) showed a clear upward trend in E15.5 *Qpct*$^{-/-}$ placentae compared to in *Qpct*$^{+/+}$ placentae in our single-cell transcriptomic datasets. Meanwhile, reduced interactions of imprinted genes were also detected in the immune cell group. The deficiency of *Qpct* may trigger an immune response linked to angiogenesis and influence the regulation of other imprinted genes. These findings indicate that the loss of maternally expressed *Qpct* in the placenta significantly enhances angiogenesis.

The "parental conflict" hypothesis proposes that paternally expressed genes promote feto-placental development, whereas maternally expressed genes act to limit fetal growth (Plagge et al., 2004; Fowden et al., 2011). Consistent with this hypothesis, the size and weight of embryos and placentae were significantly greater in *Qpct*$^{-/+}$ and *Qpct*$^{-/-}$ than in *Qpct*$^{+/+}$ and *Qpct*$^{+/-}$ mice. This indicates that maternally expressed *Qpct* genes may function to suppress embryonic and placental growth and development. A previous study reported that the imprinted gene *Mest* was associated with placental angiogenesis (Mayer et al., 2000). Further evidence has shown high expression levels of *Peg3* (a paternally expressed gene) in the human placenta, particularly in the layer of human villous cytotrophoblast cells (Hiby et al., 2001). Our results coincided with the findings of high expression of *Peg3* in the trophoblast of *Qpct*$^{+/+}$ mouse placentae (Fig. 5f). Another paternally expressed gene, *Peg10*, is also crucial for mouse placental formation, contributing to both early placental development and the maintenance of placental vasculature from mid- to late-gestation (Shiura et al., 2021). In our study, the down-regulation of six paternally imprinted genes (*Peg3*, *Igf2*, *Peg10*, *Zdbf2*, *Kcnq1ot1*, and *Dlk1*) and the overgrowth of the *Qpct*$^{-/-}$ mouse embryo and placenta are in alignment with the "parental conflict" hypothesis. In fact, all the genes described above promote growth. Moreover, multiple paternally expressed genes, such as *Igf2*, *Peg3*, and *Dlk1* (Cleaton et al., 2016; Sandovici et al., 2022), are highly expressed in feto-placental endothelial cells and promote placental angiogenesis. Therefore, their down-regulation may act as counter-regulatory mechanisms to restrict the overgrowth induced by the lack of *Qpct* expression. This is reminiscent of previous work showing that imprinted genes function within a network (Varrault et al., 2006). Our findings indicate that *Qpct* could have a significant function by modulating the expression of these paternally imprinted genes, consequently impacting the development of mouse embryos and placentae.

In the E15.5 *Qpct*$^{-/-}$ placental TGCs, up-regulated gene clusters were enriched in multiple mitochondrial and ATP metabolism pathways. These results implied that *Qpct* might alter the energy transfer by regulating the mitochondrial metabolism genes of TGCs. Overall, changes in placental mitochondrial activity are associated with fetal development (Sferruzzi-Perri et al., 2019). Additionally, prior research has demonstrated that the up-regulation of mitofusins (*Mfn1* and *Mfn2*) influences mitochondrial structure (Chen et al., 2003). *Tfam* is critical for the regulation, preservation, and structural organization of the mitochondrial genome (Ngo et al., 2011). Moreover, *Tfam* deficiency results in impaired mitochondrial function (Desdin-Mico et al., 2020), while its overexpression can ameliorate mitochondrial deficiencies (Ikeuchi et al., 2005). In our study, we observed altered mitochondrial distribution and up-regulation of *Mfn1* and *Tfam* in *Qpct*$^{-/+}$ and *Qpct*$^{-/-}$ placentae compared with those in *Qpct*$^{+/+}$ and *Qpct*$^{+/-}$ placentae. Overall, we speculate that the absence of the *Qpct* allele could cause excessive energy transfer to embryos, resulting in mitochondrial dysfunction.

Previous studies have shown that *Lrg1* could promote angiogenesis by up-regulating the expression of *TGF-β* in endothelial cells (Wang et al., 2013). ANGPTL4 functions as a versatile secretory protein, while VEGF plays a key role in promoting angiogenesis (Guo et al., 2014). In addition, *MIF* may stimulate angiogenesis by up-regulating the expression of *VEGF*, *IL8*, and *MCP1* (Veillat et al., 2010). Based on this evidence, we focused on angiogenesis-associated gene clusters (*Lrg1*, *TGF-β*, *VEGF*, *ANGPTL*, *MIF*, *MCP-1*, *IL6*, and *IL8*) and found that their expression was significantly increased in E15.5 *Qpct*$^{-/-}$ placentae. Specifically, *VEGFβ* and *PIGF* could bind *VEGFR1* and affect vascular permeability by inducing macrophages to produce pro-inflammatory factors (Uemura et al., 2021). *Mif* activates *Cd74* (Pantouris et al., 2018; Parkins et al., 2021), *Cd44* (Veillat et al., 2010), and *Ackr3* (van der Vorst et al., 2015), leading to the production of inflammatory and major angiogenic factors. *Mdk*

can induce stratification of endothelial cells and induce angiogenesis (Sumi et al., 2002; Weckbach et al., 2012). Consistent with these results, the specific ligand–receptor pairs mentioned above (*VEGFB–VEGFR1*, *Mif–Ackr3*, *Mif–Cd74*, and *Mif–Cd44*) were increased in E15.5 *Qpct*$^{-/-}$ placentae in our study (Figs. 7a, 7d, and 7e). This finding suggests that these ligand–receptor pairs may affect the process of angiogenesis in *Qpct*$^{-/-}$ mouse placentae. In summary, our results indicate that *Qpct* is an angiogenesis-inhibiting factor, offering potential new perspectives for the treatment of angiogenesis-related diseases in the future.

Data availability statement

The single-cell sequencing datasets have been deposited in the Gene Expression Omnibus (GEO) database under the accession number GSE189103. Additional supplementary data are available in the article and supplementary files.

Acknowledgments

This work was supported by the National Natural Science Foundation of China (No. 32271165) and the Interdisciplinary Project in Ocean Research of Tongji University (No. 2022-2-ZD-02), China. Dr. Xu WANG did not receive any funding from the grant agencies mentioned above.

Author contributions

Jing GUO, Ruixia LI, Jindong YAO, and He ZHANG conducted the experiments and sequencing (including the breeding and identification of *Qpct* model mice). Jing GUO and Jihong ZHENG performed the bioinformatic analyses. Jing GUO, Xu WANG, and Chao ZHANG wrote the manuscript. Xu WANG and Chao ZHANG supervised and coordinated all aspects of the research. All authors have read and approved the final manuscript, and therefore, have full access to all the data in the study and take responsibility for the integrity and security of the data.

Compliance with ethics guidelines

Jing GUO, Jihong ZHENG, Ruixia LI, Jindong YAO, He ZHANG, Xu WANG, and Chao ZHANG declare that they have no conflicts of interest.

All animal procedures were approved by the Institutional Animal Care and Use Committees (IACUC) of Tongji University (Approval No. TJAB05221102).

References

Abu El-Asrar AM, Ahmad A, Siddiquei MM, et al., 2019. The proinflammatory and proangiogenic macrophage migration inhibitory factor is a potential regulator in proliferative diabetic retinopathy. *Front Immunol*, 10:2752. https://doi.org/10.3389/fimmu.2019.02752

Arauzo-Bravo MJ, Delic D, Gerovska D, et al., 2020. Protective vaccination reshapes hepatic response to blood-stage malaria of genes preferentially expressed by NK cells. *Vaccines (Basel)*, 8(4):677. https://doi.org/10.3390/vaccines8040677

Bartolomei MS, Zemel S, Tilghman SM, 1991. Parental imprinting of the mouse H19 gene. *Nature*, 351:153-155. https://doi.org/10.1038/351153a0

Bode S, Peters C, Deussing JM, 2005. Placental cathepsin M is alternatively spliced and exclusively expressed in the spongiotrophoblast layer. *Biochim Biophys Acta*, 1731(3): 160-167. https://doi.org/10.1016/j.bbaexp.2005.10.005

Bullerwell CE, Robichaud PP, Deprez PML, et al., 2021. EBF1 drives hallmark B cell gene expression by enabling the interaction of PAX5 with the MLLH3K4 methyltransferase complex. *Sci Rep*, 11:1537. https://doi.org/10.1038/s41598-021-81000-5

Busby WH, Quackenbush GE, Humm J, et al., 1987. An enzyme(s) that converts glutaminyl-peptides into pyroglutamyl-peptides. Presence in pituitary, brain, adrenal medulla, and lymphocytes. *J Biol Chem*, 262(18):8532-8536. https://doi.org/10.1016/S0021-9258(18)47446-7

Carbone C, Piro G, Merz V, et al., 2018. Angiopoietin-like proteins in angiogenesis, inflammation and cancer. *Int J Mol Sci*, 19(2):431. https://doi.org/10.3390/ijms19020431

Charalambous M, Cowley M, Geoghegan F, et al., 2010. Maternally-inherited *Grb10* reduces placental size and efficiency. *Dev Biol*, 337(1):1-8. https://doi.org/10.1016/j.ydbio.2009.10.011

Chen H, Detmer SA, Ewald AJ, et al., 2003. Mitofusins Mfn1 and Mfn2 coordinately regulate mitochondrial fusion and are essential for embryonic development. *J Cell Biol*, 160(2):189-200. https://doi.org/10.1083/jcb.200211046

Chen M, Yi B, Zhu N, et al., 2016. Pim1 kinase promotes angiogenesis through phosphorylation of endothelial nitric oxide synthase at Ser-633. *Cardiovasc Res*, 109(1):141-150. https://doi.org/10.1093/cvr/cvv250

Cleaton MA, Dent CL, Howard M, et al., 2016. Fetus-derived DLK1 is required for maternal metabolic adaptations to pregnancy and is associated with fetal growth restriction. *Nat Genet*, 48(12):1473-1480. https://doi.org/10.1038/ng.3699

Dalangood S, Zhu Z, Ma Z, et al., 2020. Identification of glycogene-type and validation of ST3GAL6 as a biomarker predicts clinical outcome and cancer cell invasion in urinary bladder cancer. *Theranostics*, 10(22):10078-10091. https://doi.org/10.7150/thno.48711

Desdin-Mico G, Soto-Heredero G, Aranda JF, et al., 2020. T cells with dysfunctional mitochondria induce multimorbidity and premature senescence. *Science*, 368(6497):1371-1376. https://doi.org/10.1126/science.aax0860

Ding J, Adiconis X, Simmons SK, et al., 2020. Systematic comparison of single-cell and single-nucleus RNA-sequencing methods. *Nat Biotechnol*, 38:737-746. https://doi.org/10.1038/s41587-020-0465-8

Doherty AS, Mann MR, Tremblay KD, et al., 2000. Differential effects of culture on imprinted *H19* expression in the preimplantation mouse embryo. *Biol Reprod*, 62(6):1526-1535. https://doi.org/10.1095/biolreprod62.6.1526

Dunk CE, van Dijk M, Choudhury R, et al., 2021. Functional evaluation of STOX1 (STORKHEAD-BOX PROTEIN 1) in placentation, preeclampsia, and preterm birth. *Hypertension*, 77(2):475-490. https://doi.org/10.1161/HYPERTENSIONAHA.120.15619

Farmer DT, Nathan S, Finley JK, et al., 2017. Defining epithelial cell dynamics and lineage relationships in the developing lacrimal gland. *Development*, 144(13):2517-2528. https://doi.org/10.1242/dev.150789

Fearon U, Mullan R, Markham T, et al., 2006. Oncostatin M induces angiogenesis and cartilage degradation in rheumatoid arthritis synovial tissue and human cartilage cocultures. *Arthritis Rheum*, 54(10):3152-3162. https://doi.org/10.1002/art.22161

Fowden AL, Coan PM, Angiolini E, et al., 2011. Imprinted genes and the epigenetic regulation of placental phenotype. *Prog Biophys Mol Biol*, 106(1):281-288. https://doi.org/10.1016/j.pbiomolbio.2010.11.005

Garfield AS, Cowley M, Smith FM, et al., 2011. Distinct physiological and behavioural functions for parental alleles of imprinted *Grb10*. *Nature*, 469:534-538. https://doi.org/10.1038/nature09651

Guo J, He H, Liu Q, et al., 2015. Identification and epigenetic analysis of a maternally imprinted gene *Qpct*. *Mol Cells*, 38(10):859-865. https://doi.org/10.14348/molcells.2015.0098

Guo L, Li SY, Ji FY, et al., 2014. Role of Angptl4 in vascular permeability and inflammation. *Inflamm Res*, 63(1):13-22. https://doi.org/10.1007/s00011-013-0678-0

Haig D, 2014. Coadaptation and conflict, misconception and muddle, in the evolution of genomic imprinting. *Heredity (Edinb)*, 113(2):96-103. https://doi.org/10.1038/hdy.2013.97

Halari CD, Nandi P, Jeyarajah MJ, et al., 2020. Decorin production by the human decidua: role in decidual cell maturation. *Mol Hum Reprod*, 26(10):784-796. https://doi.org/10.1093/molehr/gaaa058

Hemberger M, Hanna CW, Dean W, 2020. Mechanisms of early placental development in mouse and humans. *Nat Rev Genet*, 21:27-43. https://doi.org/10.1038/s41576-019-0169-4

Hiby SE, Lough M, Keverne EB, et al., 2001. Paternal monoallelic expression of *PEG3* in the human placenta. *Hum Mol Genet*, 10(10):1093-1100. https://doi.org/10.1093/hmg/10.10.1093

Hong J, Qu P, Wuest TR, et al., 2019. Neutrophilic granule protein is a novel murine LPS antagonist. *Immune Netw*, 19(5):e34. https://doi.org/10.4110/in.2019.19.e34

Hou J, Zhang J, Cui P, et al., 2021. TREM2 sustains macrophage-hepatocyte metabolic coordination in nonalcoholic fatty liver disease and sepsis. *J Clin Invest*, 131(4):e135197. https://doi.org/10.1172/JCI135197

Hu W, Chien SY, Ying P, et al., 2020. Impact of *CCL4* gene polymorphisms upon the progression of lung cancer in a Han Chinese cohort. *Medicine (Baltimore)*, 99(3):e18906. https://doi.org/10.1097/MD.0000000000018906

Ikeuchi M, Matsusaka H, Kang D, et al., 2005. Overexpression of mitochondrial transcription factor A ameliorates mitochondrial deficiencies and cardiac failure after myocardial infarction. *Circulation*, 112(5):683-690. https://doi.org/10.1161/CIRCULATIONAHA.104.524835

Jaipersad AS, Lip GY, Silverman S, et al., 2014. The role of monocytes in angiogenesis and atherosclerosis. *J Am Coll Cardiol*, 63(1):1-11. https://doi.org/10.1016/j.jacc.2013.09.019

Jaitin DA, Adlung L, Thaiss CA, et al., 2019. Lipid-associated macrophages control metabolic homeostasis in a Trem2-dependent manner. *Cell*, 178(3):686-698.e14. https://doi.org/10.1016/j.cell.2019.05.054

Jakubzick CV, Randolph GJ, Henson PM, 2017. Monocyte differentiation and antigen-presenting functions. *Nat Rev Immunol*, 17(6):349-362. https://doi.org/10.1038/nri.2017.28

Jiao B, Liu S, Tan X, et al., 2021. Class-3 semaphorins: potent multifunctional modulators for angiogenesis-associated diseases. *Biomed Pharmacother*, 137:111329. https://doi.org/10.1016/j.biopha.2021.111329

Jin S, Guerrero-Juarez CF, Zhang L, et al., 2021. Inference and analysis of cell-cell communication using CellChat. *Nature Communications*, 12:1088. https://doi.org/10.1038/s41467-021-21246-9

Korkolopoulou P, Cordell J, Jones M, et al., 1994. The expression of the B-cell marker mb-1 (CD79a) in Hodgkin's disease. *Histopathology*, 24(6):511-515. https://doi.org/10.1111/j.1365-2559.1994.tb00568.x

Kuo CY, Shevchuk M, Opfermann J, et al., 2019. Trophoblast-endothelium signaling involves angiogenesis and apoptosis in a dynamic bioprinted placenta model. *Biotechnol Bioeng*, 116(1):181-192. https://doi.org/10.1002/bit.26850

Larson SR, Atif SM, Gibbings SL, et al., 2016. Ly6C$^+$ monocyte efferocytosis and cross-presentation of cell-associated antigens. *Cell Death Differ*, 23(6):997-1003. https://doi.org/10.1038/cdd.2016.24

Li TJ, Jiang YM, Hu YF, et al., 2017. Interleukin-17-producing neutrophils link inflammatory stimuli to disease progression by promoting angiogenesis in gastric cancer. *Clin Cancer Res*, 23(6):1575-1585. https://doi.org/10.1158/1078-0432.CCR-16-0617

Li WV, Li Y, 2021. ScLink: inferring sparse gene co-expression networks from single-cell expression data. *Genomics Proteomics Bioinformatics*, 19(3):475-492. https://doi.org/10.1016/j.gpb.2020.11.006

Liao YY, Tsai HC, Chou PY, et al., 2016. CCL3 promotes angiogenesis by dysregulation of miR-374b/VEGF-A axis in human osteosarcoma cells. *Oncotarget*, 7(4):4310-4325. https://doi.org/10.18632/oncotarget.6708

Liu Y, Fan X, Wang R, et al., 2018. Single-cell RNA-seq reveals the diversity of trophoblast subtypes and patterns of differentiation in the human placenta. *Cell Res*, 28(8):819-832.

https://doi.org/10.1038/s41422-018-0066-y

Mann MR, Lee SS, Doherty AS, et al., 2004. Selective loss of imprinting in the placenta following preimplantation development in culture. *Development*, 131(15):3727-3735. https://doi.org/10.1242/dev.01241

Marsh B, Blelloch R, 2020. Single nuclei RNA-seq of mouse placental labyrinth development. *Elife*, 9:e60266. https://doi.org/10.7554/eLife.60266

Mayer W, Hemberger M, Frank HG, et al., 2000. Expression of the imprinted genes *MEST*/*Mest* in human and murine placenta suggests a role in angiogenesis. *Dev Dyn*, 217(1):1-10. https://doi.org/10.1002/(SICI)1097-0177(200001)217:1%3C1::AID-DVDY1%3E3.0.CO;2-4

McCoy MG, Nascimento DW, Veleeparambil M, et al., 2021. Endothelial TLR2 promotes proangiogenic immune cell recruitment and tumor angiogenesis. *Sci Signal*, 14(666):eabc5371. https://doi.org/10.1126/scisignal.abc5371

McDonald LE, Paterson CA, Kay GF, 1998. Bisulfite genomic sequencing-derived methylation profile of the *Xist* gene throughout early mouse development. *Genomics*, 54(3):379-386. https://doi.org/10.1006/geno.1998.5570

Medaglia C, Giladi A, Stoler-Barak L, et al., 2017. Spatial reconstruction of immune niches by combining photoactivatable reporters and scRNA-seq. *Science*, 358(6370):1622-1626. https://doi.org/10.1126/science.aao4277

Menezes S, Melandri D, Anselmi G, et al., 2016. The heterogeneity of Ly6C^{hi} monocytes controls their differentiation into iNOS^{+} macrophages or monocyte-derived dendritic cells. *Immunity*, 45(6):1205-1218. https://doi.org/10.1016/j.immuni.2016.12.001

Miozzo M, Grati FR, Bulfamante G, et al., 2001. Post-zygotic origin of complete maternal chromosome 7 isodisomy and consequent loss of placental *PEG1*/*MEST* expression. *Placenta*, 22(10):813-821. https://doi.org/10.1053/plac.2001.0728

Moncho-Amor V, Ibanez de Caceres I, Bandres E, et al., 2011. DUSP1/MKP1 promotes angiogenesis, invasion and metastasis in non-small-cell lung cancer. *Oncogene*, 30(6):668-678. https://doi.org/10.1038/onc.2010.449

Moussad EE, Rageh MA, Wilson AK, et al., 2002. Temporal and spatial expression of connective tissue growth factor (CCN2; CTGF) and transforming growth factor β type 1 (TGF-β1) at the utero-placental interface during early pregnancy in the pig. *Mol Pathol*, 55(3):186-192. https://doi.org/10.1136/mp.55.3.186

Nelson AC, Mould AW, Bikoff EK, et al., 2016. Single-cell RNA-seq reveals cell type-specific transcriptional signatures at the maternal-foetal interface during pregnancy. *Nat Commun*, 7:11414. https://doi.org/10.1038/ncomms11414

Ngo HB, Kaiser JT, Chan DC, 2011. The mitochondrial transcription and packaging factor Tfam imposes a U-turn on mitochondrial DNA. *Nat Struct Mol Biol*, 18(11):1290-1296. https://doi.org/10.1038/nsmb.2159

Okae H, Hiura H, Nishida Y, et al., 2012. Re-investigation and RNA sequencing-based identification of genes with placenta-specific imprinted expression. *Hum Mol Genet*, 21(3):548-558. https://doi.org/10.1093/hmg/ddr488

Olsson A, Venkatasubramanian M, Chaudhri VK, et al., 2016. Single-cell analysis of mixed-lineage states leading to a binary cell fate choice. *Nature*, 537(7622):698-702. https://doi.org/10.1038/nature19348

Outhwaite JE, McGuire V, Simmons DG, 2015. Genetic ablation of placental sinusoidal trophoblast giant cells causes fetal growth restriction and embryonic lethality. *Placenta*, 36(8):951-955. https://doi.org/10.1016/j.placenta.2015.05.013

Pantouris G, Ho J, Shah D, et al., 2018. Nanosecond dynamics regulate the MIF-induced activity of CD74. *Angew Chem Int Ed Engl*, 57(24):7116-7119. https://doi.org/10.1002/anie.201803191

Parkins A, Skeens E, McCallum CM, et al., 2021. The N-terminus of MIF regulates the dynamic profile of residues involved in CD74 activation. *Biophys J*, 120(18):3893-3900. https://doi.org/10.1016/j.bpj.2021.08.025

Peters J, 2014. The role of genomic imprinting in biology and disease: an expanding view. *Nat Rev Genet*, 15(8):517-530. https://doi.org/10.1038/nrg3766

Picton LD, Bertuzzi M, Pallucchi I, et al., 2021. A spinal organ of proprioception for integrated motor action feedback. *Neuron*, 109(7):1188-1201.e7. https://doi.org/10.1016/j.neuron.2021.01.018

Pique-Regi R, Romero R, Tarca AL, et al., 2019. Single cell transcriptional signatures of the human placenta in term and preterm parturition. *Elife*, 8:e52004. https://doi.org/10.7554/eLife.52004

Plagge A, Gordon E, Dean W, et al., 2004. The imprinted signaling protein XLαs is required for postnatal adaptation to feeding. *Nat Genet*, 36(8):818-826. https://doi.org/10.1038/ng1397

Plasschaert RN, Bartolomei MS, 2015. Tissue-specific regulation and function of Grb10 during growth and neuronal commitment. *Proc Natl Acad Sci USA*, 112(22):6841-6847. https://doi.org/10.1073/pnas.1411254111

Prissette M, El-Maarri O, Arnaud D, et al., 2001. Methylation profiles of DXPas34 during the onset of X-inactivation. *Hum Mol Genet*, 10(1):31-38. https://doi.org/10.1093/hmg/10.1.31

Sandovici I, Georgopoulou A, Perez-Garcia V, et al., 2022. The imprinted *Igf2-Igf2r* axis is critical for matching placental microvasculature expansion to fetal growth. *Dev Cell*, 57(1):63-79.e8. https://doi.org/10.1016/j.devcel.2021.12.005

Sasaki H, Kurotaki D, Tamura T, 2016. Regulation of basophil and mast cell development by transcription factors. *Allergol Int*, 65(2):127-134. https://doi.org/10.1016/j.alit.2016.01.006

Sferruzzi-Perri AN, Higgins JS, Vaughan OR, et al., 2019. Placental mitochondria adapt developmentally and in

response to hypoxia to support fetal growth. *Proc Natl Acad Sci USA*, 116(5):1621-1626. https://doi.org/10.1073/pnas.1816056116

Shiura H, Ono R, Tachibana S, et al., 2021. Peg10 viral aspartic protease domain is essential for the maintenance of fetal capillary structure in the mouse placenta. *Development*, 148(19):dev199564. https://doi.org/10.1242/dev.199564

Singh H, Endo Y, Nie G, 2011. Decidual HtrA3 negatively regulates trophoblast invasion during human placentation. *Hum Reprod*, 26(4):748-757. https://doi.org/10.1093/humrep/der019

Slyper M, Porter CBM, Ashenberg O, et al., 2020. A single-cell and single-nucleus RNA-seq toolbox for fresh and frozen human tumors. *Nat Med*, 26(5):792-802. https://doi.org/10.1038/s41591-020-0844-1

Stoeckius M, Hafemeister C, Stephenson W, et al., 2017. Simultaneous epitope and transcriptome measurement in single cells. *Nat Methods*, 14(9):865-868. https://doi.org/10.1038/nmeth.4380

Strickland LA, Jubb AM, Hongo JA, et al., 2005. Plasmalemmal vesicle-associated protein (PLVAP) is expressed by tumour endothelium and is upregulated by vascular endothelial growth factor-A (VEGF). *J Pathol*, 206(4):466-475. https://doi.org/10.1002/path.1805

Sullivan BM, Liang HE, Bando JK, et al., 2011. Genetic analysis of basophil function *in vivo*. *Nat Immunol*, 12(6):527-535. https://doi.org/10.1038/ni.2036

Sumi Y, Muramatsu H, Takei Y, et al., 2002. Midkine, a heparin-binding growth factor, promotes growth and glycosaminoglycan synthesis of endothelial cells through its action on smooth muscle cells in an artificial blood vessel model. *J Cell Sci*, 115(Pt 13):2659-2667. https://doi.org/10.1242/jcs.115.13.2659

Suryawanshi H, Morozov P, Straus A, et al., 2018. A single-cell survey of the human first-trimester placenta and decidua. *Sci Adv*, 4(10):eaau4788. https://doi.org/10.1126/sciadv.aau4788

Thomas JR, Appios A, Zhao X, et al., 2021. Phenotypic and functional characterization of first-trimester human placental macrophages, Hofbauer cells. *J Exp Med*, 218(1): e20200891. https://doi.org/10.1084/jem.20200891

Torres A, Gubbiotti MA, Iozzo RV, 2017. Decorin-inducible Peg3 evokes Beclin 1-mediated autophagy and Thrombospondin 1-mediated angiostasis. *J Biol Chem*, 292(12): 5055-5069. https://doi.org/10.1074/jbc.M116.753632

Trzebanski S, Jung S, 2020. Plasticity of monocyte development and monocyte fates. *Immunol Lett*, 227:66-78. https://doi.org/10.1016/j.imlet.2020.07.007

Tucci V, Isles AR, Kelsey G, et al., 2019. Genomic imprinting and physiological processes in mammals. *Cell*, 176(5): 952-965. https://doi.org/10.1016/j.cell.2019.01.043

Tunster SJ, van de Pette M, John RM, 2011. Fetal overgrowth in the *Cdkn1c* mouse model of Beckwith-Wiedemann syndrome. *Dis Model Mech*, 4(6):814-821. https://doi.org/10.1242/dmm.007328

Tunster SJ, Creeth HDJ, John RM, 2016. The imprinted *Phlda2* gene modulates a major endocrine compartment of the placenta to regulate placental demands for maternal resources. *Dev Biol*, 409(1):251-260. https://doi.org/10.1016/j.ydbio.2015.10.015

Uemura A, Fruttiger M, D'Amore PA, et al., 2021. VEGFR1 signaling in retinal angiogenesis and microinflammation. *Prog Retin Eye Res*, 84:100954. https://doi.org/10.1016/j.preteyeres.2021.100954

van der Vorst EP, Doring Y, Weber C, 2015. MIF and CXCL12 in cardiovascular diseases: functional differences and similarities. *Front Immunol*, 6:373. https://doi.org/10.3389/fimmu.2015.00373

Varrault A, Gueydan C, Delalbre A, et al., 2006. Zac1 regulates an imprinted gene network critically involved in the control of embryonic growth. *Dev Cell*, 11(5):711-722. https://doi.org/10.1016/j.devcel.2006.09.003

Veillat V, Carli C, Metz CN, et al., 2010. Macrophage migration inhibitory factor elicits an angiogenic phenotype in human ectopic endometrial cells and triggers the production of major angiogenic factors via CD44, CD74, and MAPK signaling pathways. *J Clin Endocrinol Metab*, 95(12):E403-412. https://doi.org/10.1210/jc.2010-0417

Vento-Tormo R, Efremova M, Botting RA, et al., 2018. Single-cell reconstruction of the early maternal-fetal interface in humans. *Nature*, 563:347-353. https://doi.org/10.1038/s41586-018-0698-6

Wang XM, Abraham S, McKenzie JAG, et al., 2013. LRG1 promotes angiogenesis by modulating endothelial TGF-β signalling. *Nature*, 499(7458):306-311. https://doi.org/10.1038/nature12345

Weckbach LT, Groesser L, Borgolte J, et al., 2012. Midkine acts as proangiogenic cytokine in hypoxia-induced angiogenesis. *Am J Physiol Heart Circ Physiol*, 303(4):H429-438. https://doi.org/10.1152/ajpheart.00934.2011

Xu B, Chen X, Ding Y, et al., 2020. Abnormal angiogenesis of placenta in progranulindeficient mice. *Mol Med Rep*, 22(4):3482-3492. https://doi.org/10.3892/mmr.2020.11438

Xu Y, Luo X, Fang Z, et al., 2018. Transcription coactivator cited1 acts as an inducer of trophoblast-like state from mouse embryonic stem cells through the activation of bmp signaling. *Cell Death Dis*, 9(9):924. https://doi.org/10.1038/s41419-018-0991-1

Yan J, Gao Y, Lin S, et al., 2021. EGR1-CCL2 feedback loop maintains epithelial-mesenchymal transition of cisplatin-resistant gastric cancer cells and promotes tumor angiogenesis. *Dig Dis Sci*, 67:3702-3713. https://doi.org/10.1007/s10620-021-07250-5

Zhang X, Lan Y, Xu J, et al., 2019. Cellmarker: a manually curated resource of cell markers in human and mouse. *Nucleic Acids Res*, 47(D1):D721-D728. https://doi.org/10.1093/nar/gky900

Supplementary information

Tables S1 and S2; Fig. S1